2018-2019
AIAA/Cessna/Raytheon
Design Build Fly

University of California Irvine

Table of Contents

1. Executive Summary
2. Management Summary
  2.1 Team Organization
  2.2 Milestone Chart
3. Conceptual Design
  3.1 Mission Sequence
    3.1.1 Mission 1 - “Delivery Mission”
    3.1.2 Mission 2 - “Reconnaissance”
    3.1.3 Mission 3 - “Attack Mission”
    3.1.4 Ground Mission
  3.2 Scoring Formula
  3.3 Design Constraints
  3.4 Sensitivity Analysis
    3.4.1 Extreme Cases
  3.5 Design Requirements
  3.6 Overall System Configuration
  3.7 Subsystem Configuration
    3.7.1 Motor Configuration
    3.7.2 Empennage
    3.7.3 Landing Gear
    3.7.4 Wing Folding
    3.7.5 Store Drop Mechanism
  3.8 Conceptual Design Summary
4. Preliminary Design
  4.1 Design Methodology
    4.1.1 Mission Model
  4.2 Trade Analysis
  4.3 Sizing and Design Trades
    4.3.1 Aerodynamic Trade-Offs
    4.3.2 Propulsion Trade-Offs
    4.3.3 Final Optimized Aircraft
  4.4 Lift, Drag, and Stability Characteristics
    4.4.1 Stability and Control
  4.5 Predicted Mission Performance
5. Detailed Design
  5.1 Design Parameters

5.2 Structural Characteristics
5.3 System Design and Component Selection/Integration
5.3.1 Wing
5.3.2 Folding Mechanism
5.3.3 Locking Mechanism
5.3.4 Store Drop Mechanism
5.3.5 Tail Hook
5.3.6 Radome
5.3.7 Fuselage Boom
5.3.8 Motor Mount
5.3.9 Electronic Speed Control
5.3.10 Control Surface
5.3.11 Servo Selection
5.3.12 Landing Gear
5.4 Weight and Balance
5.5 Drawing Package
6. Manufacturing Plan
6.1 Manufacturing Processes Investigated
6.2 Manufacturing Processes Selection
6.2.1 Wings
6.2.2 Folding Mechanism
6.2.3 Locking Mechanism
6.2.4 Radome
6.2.5 Radome Attachment
6.2.6 Landing Gear
6.2.7 Store Drop Mechanism
6.2.8 Tail Hook
6.3 Manufacturing Milestone Chart
7. Testing Plan
7.1 Objectives and Schedule
7.1.1 Wing Structural Testing
7.1.2 Tail Hook Structural Testing
7.1.3 Propulsion Testing
7.2 Pre-Flight Checklist
7.3 Flight Test Plan
8. Performance Results
8.1 Performance of Key Subsystems

8.1.1 Structural Performance
8.1.2 Propulsion Performance
8.2 Flight Test Results
9. Bibliography

Nomenclature List & Acronyms Used

WRS- Written Report Score

TMS- Total Mission Score

RAC- Rated Aircraft Cost

M1- Mission 1

M2- Mission 2

M3- Mission 3

GM- Ground Mission

CA- Cyanoacrylate Adhesive

CAD- Computer Aided Design

LRU- Line Replaceable Unit

A/AR- Aspect Ratio

LARP- Low Aspect Ratio Plate

FOM- Figure of Merit

CG- Center of Gravity

α- Angle of Attack

CLV- Coefficient of Vortex Lift

CLT- Coefficient of Total Lift

CL- Coefficient of Lift (Finite Wing)

CDp- Coefficient of Parasitic Drag

L/D- Lift-to-Drag Ratio

CLmax- Maximum Coefficient of Lift

e- Oswald Efficiency Factor

(L/D)max- Maximum Lift-to-Drag Ratio

XPS- Extruded Polystyrene

CNC- Computer Numerical Control

ABS- Acrylonitrile Butadiene Styrene

Vstall- Stall Velocity

AVL- Athena Vortex Lattice

1.0 Executive Summary

This report documents the design, analysis, manufacturing processes, and testing conducted by the University of California, Irvine (UCI) Design/Build/Fly team, for the development of their aircraft entry in the 2018-2019 American Institute of Aeronautics and Astronautics (AIAA) Textron Aviation/Raytheon Missile Systems Design/Build/Fly competition. The objective of the competition is to produce an electric remote-controlled aircraft; that will not only meet the mission requirements but will receive the highest total score: a combination of the written report score and total mission score.

The theme of this year's competition is multi-purpose carrier-based aircraft. All flight missions begin with the aircraft remotely deployed from a stowed position and require takeoff from a 10-foot ramp. The aircraft must have folding surfaces and pass through a 3'x2' frame. There are two types of payloads that must be carried: a modular 12" radome capable of remote-controlled operation and external stores carried beneath the wing and fuselage that can be remotely dropped in flight. The aircraft must be capable of completing a ground mission as well as three flight missions. The flight missions will test the aircraft's performance speed, range, and efficiency when releasing a store each lap. The ground mission demonstrates the crewmembers' and pilot's ability to load & demonstrate the radome operation as well as load the stores as fast as possible. The objective of each flight mission is as follows: fly 3 demonstration laps in 5 minutes, fly 3 times laps as fast as possible within 5 minutes, and fly with & deploy as many stores as possible per lap within 10 minutes.

It was determined through a score analysis that the winning aircraft would be one that take off with & deploy as many stores as possible. The main challenge is balancing between speed, range, and power. The propulsion system would have to be optimized in finding a motor, battery, and propeller combination that provided enough thrust for takeoff and have the necessary energy onboard to maintain speed to fly the necessary laps, within 10 minutes, for Mission 3. After conducting numerous trade studies on various aircraft configurations, a conventional design with a single tractor motor was chosen.

With maximized performance in mind, the team selected a low kV motor and opted to increase the voltage and propeller diameters for each mission to gain enough thrust for takeoff while. The battery pack was sized accordingly to provide enough energy for all missions while minimizing weight. The aircraft wing was sized to maximize the amount of wing area that still could be stowed while having only one folding joint on each wing half. Constraints created by the locking and folding mechanisms drove the structural design of the main wing and landing gear sections, as well as the integration of the store drop mechanisms.

The aircraft was thoroughly ground, and flight tested to determine performance limits, optimize the propulsion system and improve the structural design though numerous design iterations. Test fights with a Pixhawk autopilot system was conducted to create controlled, repeatable propulsion evaluations holding constant course, altitude, and speed to refine and integrate power and drag values. The result is an aircraft capable of satisfying all mission objectives.

2.0 Management Summary:

The UCI team implemented an organizational structure and design timeline that focused on maximizing efficiency and team collaboration.

2.1 Team Organization

The UCI team utilizes a tiered hierarchy consisting of management, sub-teams, and individual members. Fig. 2.1 highlights the team organization employed for the 2018-19 DBF competition.

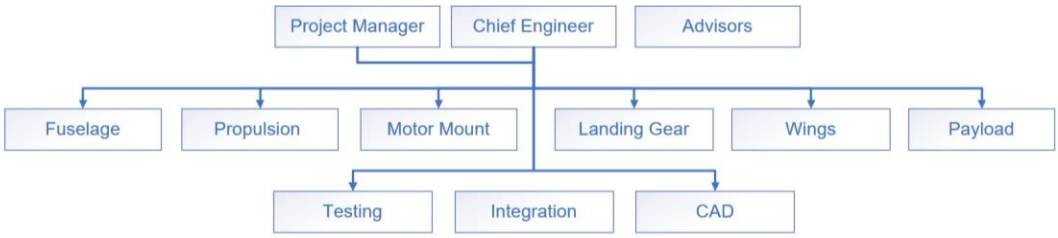

Figure 2.1: Tiered hierarchy of team management for 2018-2019 Design/Build/Fly team.

The management level consists of the chief engineer, the project manager, and advisors. The chief engineer oversees the technical side of the project. Deep understanding of the fundamentals such as driving aircraft sizing, aerodynamics, structural design, and component manufacturing techniques are necessary skills for the chief engineer to lead the overall technical direction of the aircraft. The project manager guides the direction of the team and is responsible for organization, the scheduling of major milestones (outlined in *Figure 2.2*), and resource management. The project manager conducts meetings and updates the team on needed tasks and requirements. The technical and leadership skills of management are facilitated with faculty and graduate advisors, who provide technical and professional support.

Sub-teams are responsible for designing, manufacturing, and testing their respective systems. Each sub team is led by an individual lead who is responsible for the design, manufacturing, and testing of their respective subcomponent.

- *Fuselage Team:* Designs and builds the fuselage fairings
- *Propulsion:* Tests various types of battery packs to determine the best motor-propeller combinations
- *Motor Mount:* Focuses on mounting the motor to the aircraft
- *Landing Gear:* Designs and constructs landing gear with carbon tubes and 3D printing
- *Wings:* Manages the construction of the wing with laser cutting and 3D printing
- *Payload:* Integrates and designs the attack stores and its respective drop mechanisms as well as the rotating radome
- *Testing:* Fabricates test apparatuses and conducts load testing for manufactured parts while collecting data for documentation purposes
- *Integration:* Integrates all sub-assemblies into the final aircraft

- *CAD:* Designs detailed CAD model drawings of the components of the aircraft system and helps visualize possible aircraft solutions

The team held a large-scale recruitment event at the beginning of the year to attract new members to satisfy the 1/3 underclassmen rule. New members were placed under the supervision of various team leaders and tasked with learning manufacturing processes as well as their respective team's duties and objectives. The team benefits from the enthusiasm and wealth of fresh ideas from new members as well as the experience from returning members.

2.2 Milestone Chart

Due to the demand for a competitive aircraft, an organized schedule was set up at the beginning of the year with the use of a Gantt chart. Currently, the team follows closely with the planned schedule. The project manager maintained a master schedule that tracks the various phases of the design, testing, and important milestones of the project. The planned and actual schedules are shown in *Figure 2.2*.

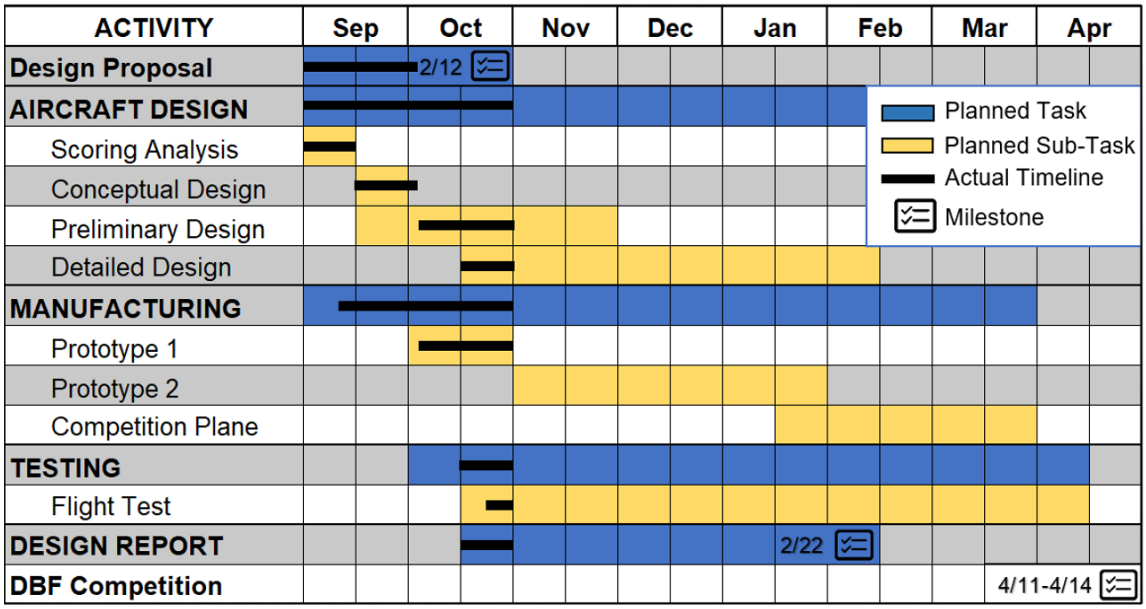

Figure 2.2: Management Gantt Chart 2018-2019

3.0 Conceptual Design

The objective of the conceptual design process is to conceptualize possible solutions that will satisfy the given competition requirements. Possible solutions are compared and analyzed using figures of merit (FOM) extracted from the analysis of the mission goals, requirements, and the design constraints provided in the contest rules. The result of this process is a combination of designs that maximize the overall flight score.

3.1 Mission Sequence

The mission sequence consists of three flight missions and one ground mission. The course consists of a 2500ft - 3500ft route with two 180° turns and one 360° turn, as shown in *Figure 3.1*. The aircraft must be capable of performing all missions and cannot begin a new mission attempt until the previous one has been successfully completed. The maximum load capability will be recorded during tech inspection and cannot be altered thereafter.

All missions must begin by entering the staging box with the aircraft in the stowed configuration. The aircraft must then be remotely commanded into its flight configuration. A wingtip test will be conducted with the largest intended payload to check the structure and locking mechanisms. The crew members will only be allowed 5-minutes to perform the deployment, loading of stores and the radome, and the wingtip test. All takeoffs will be conducted from the low side of a sloped ramp 4 feet wide and 10 feet long. The aircraft will be restrained using the tail hook at startup and released on the pilot's command. The aircraft may not contact the ground beyond the high point of the ramp. In each flight mission, a successful landing is required to receive a score. Time is stopped once the aircraft passes the start finish line in the air.

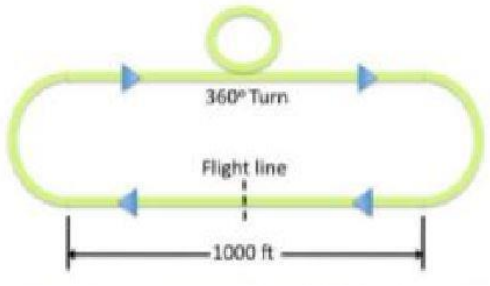

Figure 3.1: Course layout shown to scale

3.1.1 Mission 1 - "Delivery Mission"

For Mission 1, the "Delivery Mission," the aircraft, without stores or radome, must complete three laps in under five minutes. Time begins when the aircraft crosses the start/finish line in the air. A point is awarded for the successful completion of all three laps. Mission 1 scoring is indicated below:

$$\boldsymbol{M1 = 1.0}$$

3.1.2 Mission 2 - "Reconnaissance"

In Mission 2, the aircraft, with radome, must complete three timed laps in under five minutes. The radome must be remotely activated to rotate between the first and last 180 degree turns of flight. Its rotation must be clearly visible from the ground. Time will start when the aircraft passes the start/ finish line in the air. Mission 2 scoring is indicated below:

$$\boldsymbol{M2 = 1 + \frac{Min_{time}}{N_{time}}}$$

where Min_time is the fastest time for 3 laps among all the teams.

3.1.3 Mission 3 - “Attack Mission”

For Mission 3, the “Attack Mission,” the aircraft, beginning with attack stores loaded, must remotely drop a single payload store on the downwind leg of each lap beginning after the first upwind turn. All laps are to be flown within ten minutes. A lap does not count as a scoring lap if more than one store is dropped per lap.

$$\boldsymbol{M3 = 2 + number\ of\ scoring\ laps}$$

3.1.4 Ground Mission

For the timed ground mission, only the pilot and assembly crew may participate, with only the crew members allowed to touch the aircraft. Time starts when a competition official dictates the beginning of the mission. The aircraft must be remotely commanded from its stowed configuration into flight position. The crew members must then install the radome and return to the start/finish line while the pilots demonstrate its functionality. The time stops when the crew members crosses the start/finish line and resumes when the competition official resumes the mission. Next, the crew members remove the radome, and install 4 attack stores onto the aircraft. Finally, the crew members will arm the aircraft and the pilot will demonstrate flight controls and the propulsion system. The aircraft will then be disarmed, and the store drop functionality will be demonstrated with each of the four stores being dropped individually. The ground mission scores is as follows:

$$\boldsymbol{GM = \frac{Min_{time}}{N_{time}}}$$

where Min_time is the fastest ground mission time of all teams.

3.2 Scoring Formula

The total score for the missions is computed from individual mission scores as follows:

Total Mission Score = M1 + M2 + M3 + GM

The overall competition score is computed from the total mission score and written report score as follows:

Score = Written Report Score*Total Mission Score

3.3 Design Constraints

The team analyzed the contest rules to determine meaningful design limitations set by the contest. The main requirements for the Design/Build/Fly competition for this year are as follows:

- *The front surface of the aircraft and the aft landing gear must fit within 2’*
- *The folded span and height of the aircraft must fit within a 3’x2’ box and the aircraft must be able to roll completely without interference with the box*
- *All takeoffs must be from a 10’ ramp and aircraft must not touch the ground once it leaves the ramp*

- *Must carry at least 4 stores externally on the bottom surface of the main wing and on the bottom surface of the fuselage and be unfaired*
- *There is a time limit for the three flight missions, they are 5, 5, and 10 minutes respectively.*
- *There is no limit on voltage or current*

3.4 Sensitivity Analysis

The score equations were analyzed to see the impact of each parameter on the total score. The first stage of the analysis considered extreme cases to determine unusual behavior in the scoring conditions.

3.4.1 Extreme Cases

Reasonable extreme aircraft are analyzed to see if certain variables have an extreme effect on the overall score. Each case makes use of estimates for performance and total weight. The scores for each mission are shown in *Figure 3.2*.

- **Case 1: Maximize for Ground Mission (loading time):** An aircraft which is highly optimized for the ground mission will have a maximum possible score of 1 for that mission. Additionally, it is assumed that maximizing for loading time will minimize the amount of stores carried for M3 due to physical loading constraints resulting in a score of 4 for M3. An average score of 1.5 for mission 2 results in a total score of 9.5.
- **Case 2: Maximize for Mission 2:** An aircraft optimized for Mission 2 is assumed to devote a higher percentage of its weight to propulsion and battery capacity. It is also assumed to minimize the number of stores carried for Mission 3 to reduce drag and weight resulting in a score of 4. Assuming an average score of .5 for the ground mission this results in a total score of 9.5.
- **Case 3: Maximize for Mission 3:** An aircraft optimized for Mission 3 flies with the maximum number of payloads that can be carried while maintaining takeoff capabilities and store clearance. It is assumed that its cruise speed is sufficiently high to perform well in M2 as well with a score of 1.80. Assuming little to no points for the ground mission, the total score for this scenario is: 4.5 + the number of scoring laps.

As shown in the extreme case optimizing Mission 3, only 6 stores would have to be carried to earn a better score than optimizing for any other mission. There is no peak point of performance regarding the number of stores and there is no reason to reduce performance for any other mission.

3.4 Sensitivity Analysis

The design is driven by constraints in the general aircraft requirements and the most sensitive scoring parameters. Two major assumptions are 1) the store loading time for the ground mission increases with additional store capacity due to potentially more complex store retention mechanisms and

2) aircraft with larger store capacities are expected to cruise at much higher speeds allowing for faster Mission 2 times. The sensitivity analysis shows that the score, under these assumptions, is insensitive to the ground mission time (*Figure 3.2*). The total mission score characteristically follows the Mission 3 score with an offset due to the Mission 1 score, the portion of the Mission 2 score independent of time, and the portion of the Mission 3 score independent of the number of stores. Because the score sensitivity shows a significant dependence on the Mission 3 score, the number of stores carried drove preliminary design decisions.

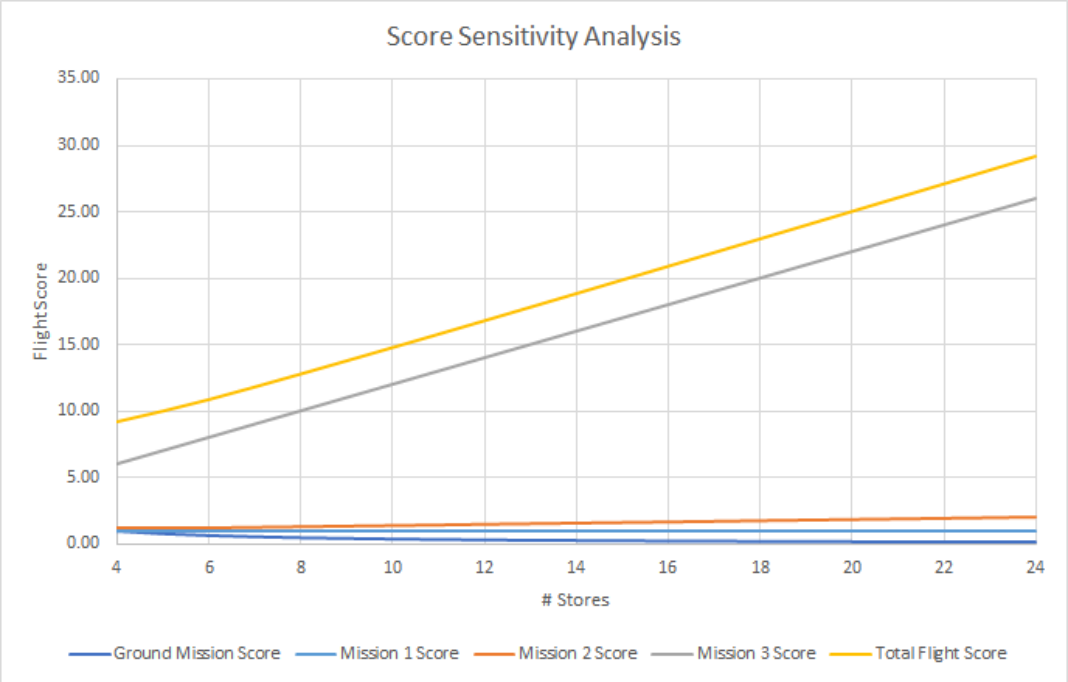

Figure 3.2: Score Sensitivity Analysis graph

3.5 Design Requirements

The sensitivity analysis concluded the following, in descending order of importance: Mission 3 Score, Mission 2 Score, Mission 1 Score, Ground Mission Score.

3.6 Overall System Configuration

Multiple aircraft configurations were considered and evaluated according to mission requirements resulting from the sensitivity analysis. The short field takeoff placed considerable emphasis on maximizing lift (35%) to minimize power requirements. Form factor (35%) was also carefully considered to ensure the stowed size constraint was met while minimizing the number of folding joints and mechanical parts. Given the store spacing requirements, cargo capacity (10%) was an additional consideration to maximize the number of stores that could be carried in M3. These constraints along with weight are listed and compared below with the conventional design serving as a baseline.

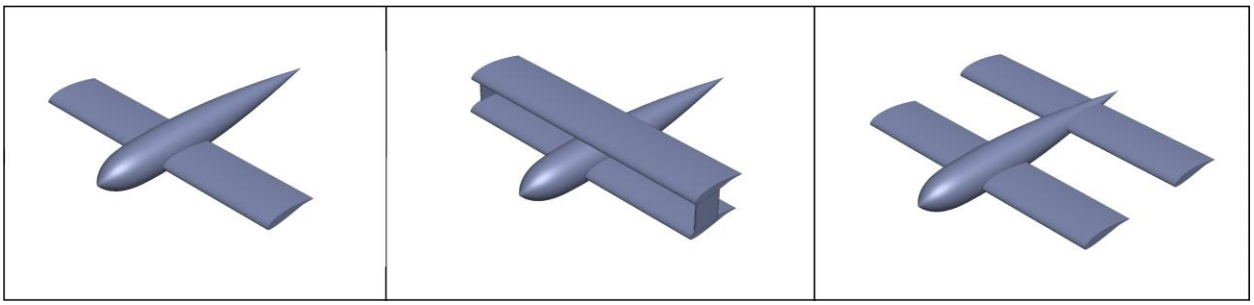

Figure 3.3: Monoplane, Biplane, and Tandem configurations

- **Monoplane:** This aircraft has stable and reliable control characteristics that are the most predictable of all designs. The single wing also requires fewer folding and locking mechanisms. Additional wing area, however, is limited without creating more than two folding surfaces.
- **Biplane:** The biplane offers the most wing area per given span. It requires, however, additional structure which would complicate the folding and locking mechanism and incur more weight.
- **Tandem:** The two wings offer more wing area per given span than the monoplane while avoiding the complexities of a biplane wing folding and locking mechanism. It would potentially, however, require more folds than a monoplane of a given wing area.

Table 3.1: Figures of Merit for overall system configuration

FOM	Weight	Monoplane	Biplane	Tandem
L/D	35	**0**	+1	+1
Form Factor	35	**0**	-1	-1
Cargo Capacity	10	**0**	-1	+1
Weight	20	**0**	-1	-1
Total	100	**0**	-30	-10

Based on the figures of merit in *Table 3.1*, a monoplane configuration was chosen. It maximizes lift while minimizing power requirements, easily meets size constraints, can carry the necessary cargo capacity, and adds the least amount of weight to the overall aircraft.

3.7 Subsystem Configuration

After the conventional system was selected the major subsystems were analyzed using their figures of merits. The following results for motor configuration, empennage, and landing gear are presented below.

3.7.1 Motor Configuration

Multiple motor configurations were considered and evaluated based on their efficiency and performance during takeoff and flight. Propeller clearance (45%) was considered the most crucial criteria due to the size restriction of the stowed aircraft. Energy efficiently (40%) was also an important factor due to the aircraft's range requirements. These are listed and compared below with the single tractor serving as a baseline.

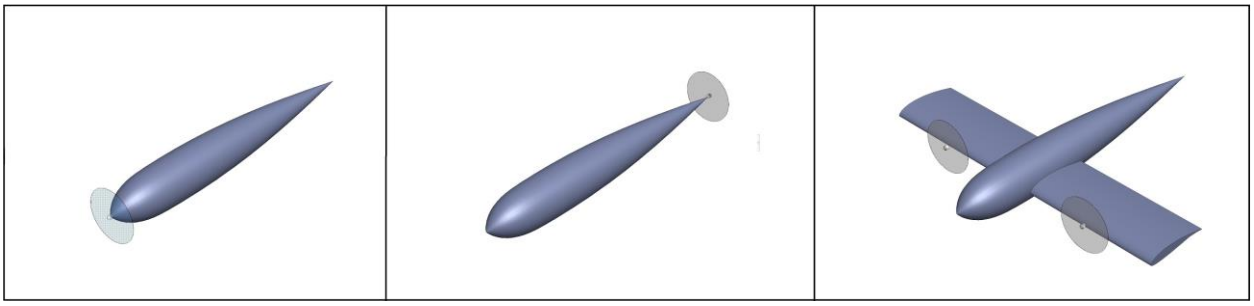

Figure 3.4: Single Tractor, Single Pusher, Double Tractor configurations

- **Single Tractor**: A tractor configuration is efficient due to the undisturbed airflow in front of the motor. The single motor configuration, however, limits propeller diameter. Additionally, the tractor configuration creates propwash for most of the aircraft.
- **Single Pusher:** A single motor aft of the aircraft would allow better air flow around the airframe. It is less efficient, however, because the propeller operates in the fuselage wake.
- **Double Tractor:** Multiple motors allow greater disc area for a given propeller diameter clearance. This configuration is less electrically efficient due to the additional branch of propellers and motors. It also incurs more weight due to the requirement of additional electronics and wiring.

FOM	Weight	Single Tractor	Double Tractor	Pusher
Propeller Clearance	45	**0**	+1	0
Efficiency	40	**0**	-1	-1
Weight	15	**0**	-1	0
Total	100	**0**	-10	-40

Table 3.2: Figures of Merit for motor configuration

According to the analysis performed in the figures of merit (*Table 3.2*), a single tractor configuration is the best configuration based upon its efficiency, weight, and ability to meet size constraints. Thus, this arrangement was chosen.

3.7.2 Empennage

Three empennage configurations are considered with conventional design as the baseline. Vertical height (30%) was considered most important due to the size constraints of the stowed aircraft configuration. Stability and control (25%) was also considered important to be able to control and sufficiently rotate the aircraft during takeoff. Weight (25%) was considered next of importance to minimize power requirements during takeoff. Manufacturing (20%) was least important in terms of empennage design.

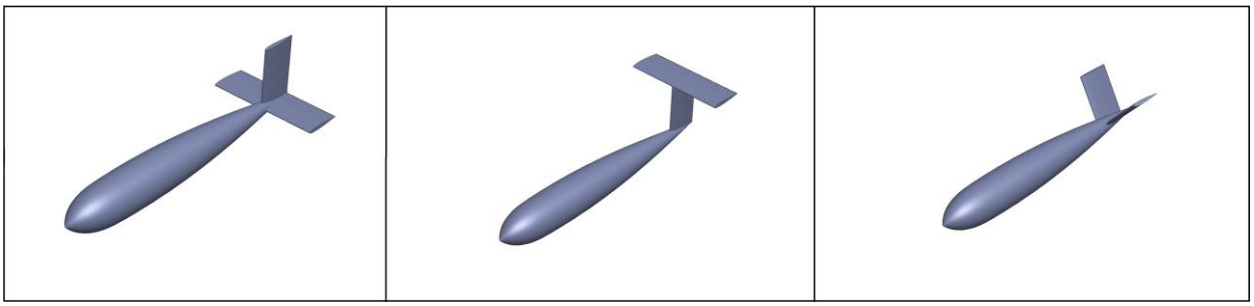

Figure 3.5: Conventional Tail, V-Tail, T-Tail configurations

- **Conventional Tail:** This conventional configuration is the most stable and a familiar design to size and to fly with. It has optimal levels of stability and control.
- **V-Tail:** A V-tail avoids clearance issue from having a tall vertical. It also potentially has less wetted area than a comparable conventional tail which reduces parasitic drag.
- **T-Tail:** Horizontal stabilizer gets clean air by joining with the vertical stabilizer on top, but adds structural weight. The T-Tail also has greater packaging difficulty.

FOM	Weight	Conventional	V-Tail	T-Tail
Vertical Height	30	**0**	1	-1
Stability and Control	25	**0**	-1	0
Weight	25	**0**	0	-1
Manufacturing Ease	20	**0**	-1	0
Total	100	**0**	-15	-55

Table 3.3 :Figures of Merit for empennage

The figures of merit in *Table 3.3* show that the conventional tail was the only configuration without a negative total. It has a favorable vertical height given the size constraints, capacity for stability and control, minimized weight, and straightforward manufacturing, which made it the ideal configuration for our design.

3.7.3 Landing Gear

Due to the nose-aft gear size constraint of the stowed aircraft, landing gear length (50%) was considered a crucial factor in its configuration selection. The landing gear also needed to provide clearance for the propeller. This potentially tall gear needed to be durable enough (25%) to withstand vertical and horizontal loads as well as bending moments. Drag (15%) is considered due to the large size gear necessary to support a heavy aircraft.

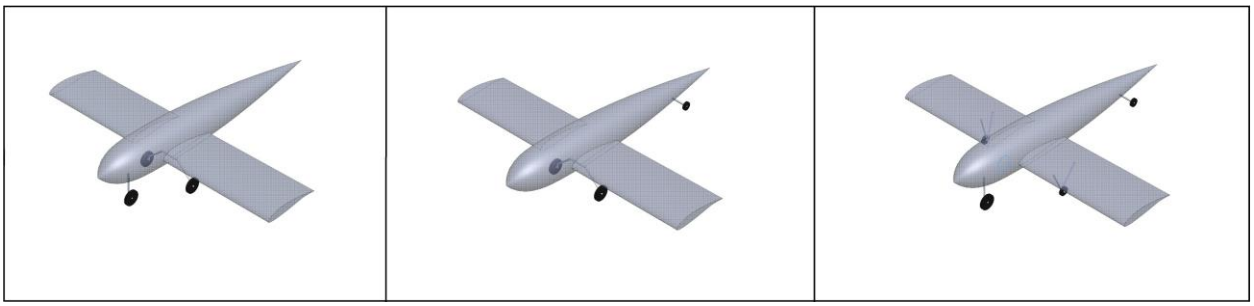

Figure 3.6: Tricycle, Tail Dragger, and Bicycle landing gear configurations

- **Tricycle:** The tricycle configuration has two main wheels under the wing aft of the aircraft CG, and a centerline nose wheel. The nose wheel is exposed to the propeller wake, causing a significant drag penalty.
- **Tail Dragger:** The tail dragger has two main wheels under the wing and one smaller wheel under the tail of the aircraft. This configuration limits the length of the aircraft due to the two foot nose to aft gear constraint. This configuration creates less additional drag and weight than the tricycle configuration.
- **Bicycle:** The bicycle has two centerline main wheels and two wing tip wheels. The landing gear structure can be reduced as the main loads are transferred through the center wheel, but the additional wheels and struts add drag.

FOM	Weight	Tricycle	Bicycle	Tail Dragger
Length	50	**+1**	-1	0
Durability	25	**-1**	0	0
Drag	15	**0**	-1	0
Weight	10	**0**	0	0
Total	100	**25**	-65	0

Table 3.4: Figures of Merit for landing gear

Given the design constraints and the objective of the landing gear, the tricycle configuration was chosen due to its benefits towards the two-foot nose to aft gear constraint (*Table 3.4*).

3.7.4 Wing Folding

Wing folding configurations were evaluated based on the force (25%) required for folding since most actuators have a limited range of force and displacement before power and weight costs become high. Structural weight (20%) and space requirements (30%) were additional factors of importance.

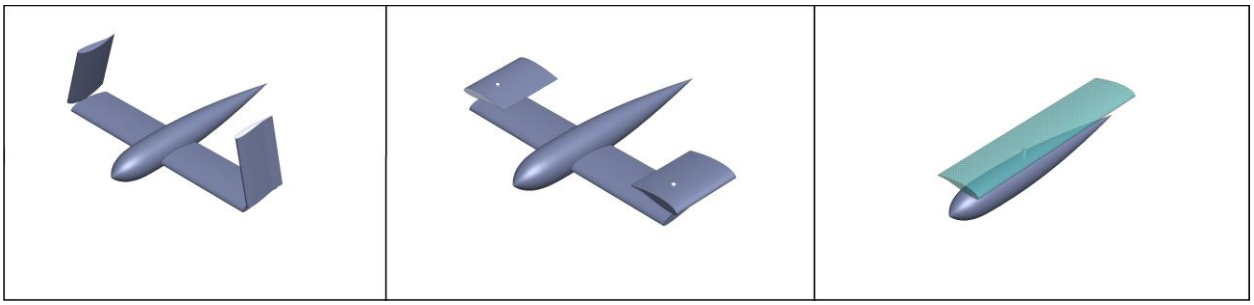

Figure 3.7: Hinge, Pivot, and Central Pivot wing folding configurations

- **Hinge:** The wing is hinged such that its folds along its span. This configuration requires more structure to carry force across the spar and requires a high amount of force to lift the wing against gravity. It is, however, the least obtrusive folding configuration.
- **Pivot:** The wing tips pivot back and rotate such that its chord line remains parallel with that of the main wing section. This configuration is better at transferring spanwise moments and avoids excessive weight of additional hinge structure.
- **Central Pivot:** The wing pivots such that its chord line is parallel the fuselage line. This configuration avoids having folds along the lifting surface. It has the least number of actuators but requires the higher folding forces which incurs a weight penalty. It also restricts the orientation of wing mounted and fuselage-based structures to allow folding clearance.

FOM	Weight	Hinge	Dual Pivot	Central Pivot
Folding Force	25	**0**	+1	0
Space Requirement	30	**0**	-1	0
Weight	20	**0**	+1	-1
Drag	25	**0**	-1	-1
Total	100	**0**	-10	-40

Table 3.5: Figures of Merit for wing folding

The FOM chart *(Table 3.5*) showed that the hinge set up was optimal as it kept the weight and drag at a minimum while requiring minimal folding force and space in order to operate compared to the dual or central pivot.

3.7.5 Store Drop Mechanism

The store drop mechanisms were evaluated on the basis of reliability (50%), ability to be consistently produced on mass (20%) and its total weight (20%). To reduce the number of wires, servomotor and radio channels used, emphasis was also placed on the efficient use of limited servos(10%).

Figure 3.8: Rail Multi Store System and Single Servo Clasp store drop mechanisms

- **Single Servo Clasp:** A single servo motor is used to control the claws holding the store in place. By sacrificing the weight of additional servos, the control of individual drop times becomes more reliable thanks to the ability to program each servo motor individually.
- **Rail Multi Store System:** A rail powered by an individual servo motor is pulled through the wing releasing the mechanisms individually. This mechanism does not require a second transmitter or microcontroller due to the small number of servos needed to implement this design. The design of this system is restricted by the folding wing design and human control of the single servo motor.

FOM	Weight	Single Servo Clasp	Rail Multi Store System
Reliability	50	**+1**	0
Manufacturability	20	**0**	0
Number of Servo Motors	10	**-1**	+1
Weight	20	**0**	0
Total	100	**40**	10

Table 3.6: Figures of Merit for store drop mechanisms

The single servo clasp configuration was selected because of its reliability in dropping one store at a time due to its ability to manage each individual store drop mechanism (*Table 3.6*). This ensures a higher chance of successfully completing scoring laps for mission 3 which is highly weighted in this year's competition.

3.8 Conceptual Design Summary

Through the conceptual design process, the finalized design chosen is a monoplane aircraft consisting of a single tractor motor coupled with a conventional tail and a tricycle landing gear. In addition

to this, the aircraft will be featuring a hinge configuration for the wing folding mechanism and a single servo clasp for the store drop mechanisms. The chosen conceptual design reflects the team's understanding of the scoring and their aim to achieve the highest possible score.

Figure 3.9: Conceptual design sketch

4.0 Preliminary Design

During preliminary design, the conceptual design configuration is refined into a solution that can complete the required tasks. This section aims to describe the process that allowed the team to converge on a suitable design. A top-level description of the design iteration flow can be observed in *Figure 4.1*. At the end of preliminary design, a high scoring aircraft began to take shape for the 2019 DBF Competition.

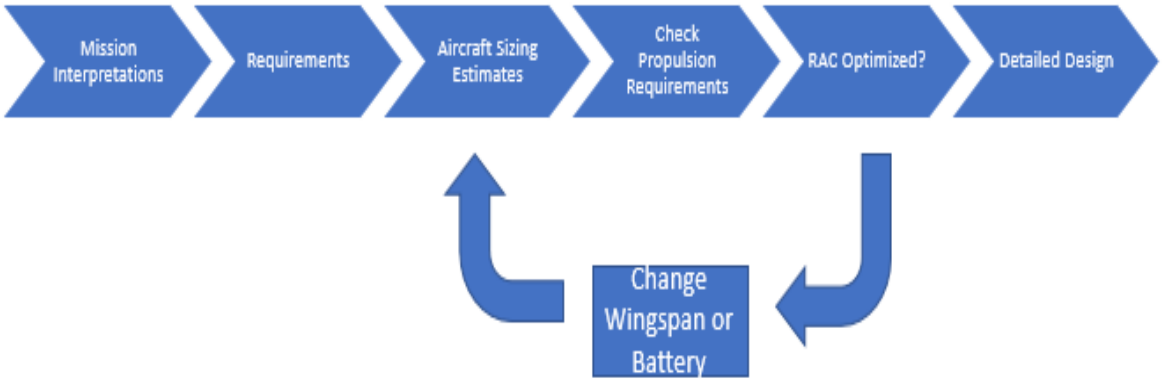

Figure 4.1: Flowchart of preliminary design process

4.1 Design Methodology

Power requirements were taken from initial drag estimations drawn from the preliminary configurations. Weight and power figures were estimated from historical competition plane data and from early testing. Because takeoff capabilities, range, and store capabilities were key considerations for the competition, propulsion became a key parameter that dictated the sizing of the aircraft as well as its finalized cargo capacity. Takeoff thrust estimates were initially calculated from kinematics and later as a function of energy density and wing loading. A drag buildup can be created based off the sizing and geometric flat plate drag coefficients of the aircraft. Battery size is then determined based off takeoff

power and endurance parameters set from a drag buildup of the plane in operation. The number of stores carried could then be estimated based on the maximum takeoff weight and maximum power available during M3.

Having established aircraft weight and wing area force loading for the wing, folding and locking mechanisms could then be bounded. As more designs become increasingly defined, previous weight and power estimated can be refined and integrated to eventually converge on a final optimized aircraft design.

4.1.1 Mission Model

The mission model estimates propulsion power and energy requirements for each aircraft during the basic segments of flight visualized in *Figure 4.2*. The mission model is primarily used to find the limits of the flight envelope for the aircraft. Three main sections of the flight are analyzed to find power and energy required - takeoff, climb out, and cruise. Important factors in sizing the battery required are the takeoff and climb out sections, these sections have high power requirements relative to cruise and landing. An Excel sheet is used to evaluate flight conditions and calculate the amount of power and energy required for the aircraft.

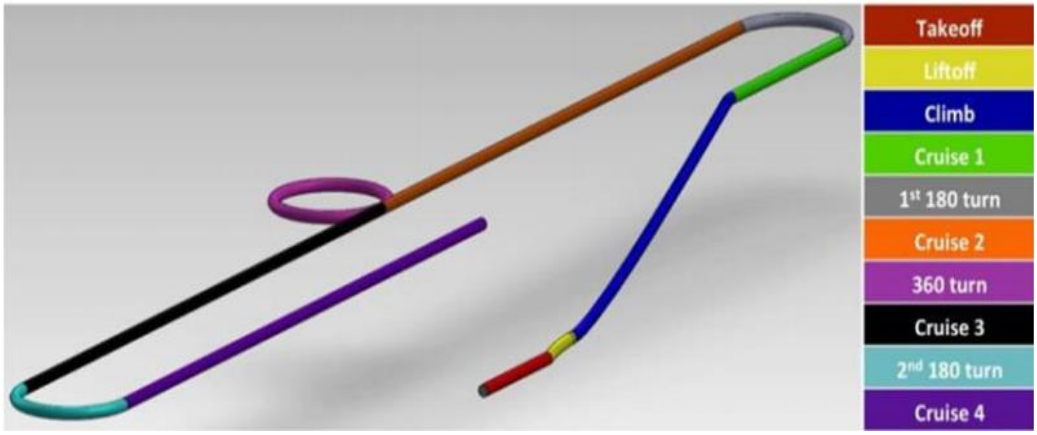

Figure 4.2: Diagram of propulsion power and energy requirements during segments of flight

Flight Segment	Constraints	Description
Takeoff	Constant angle of attack rotation when V=1.2V_stall	Aircraft accelerates on ground until rotation
Liftoff	Constant altitude	Aircraft accelerates to ideal climb sped
Climb	Constant load factor	Aircraft climbs to cruise altitude of 80-ft
Cruise	Constant Altitude	Aircraft maintains altitude
Turn	Constant load factor	Aircraft turns without overloading wings

Table 4.1: Flight segment constraints

4.2 Trade Analysis

Preliminary aircraft sizing was conducted to first estimate lift and drag requirements for the aircraft during takeoff and during operation. These early drag build ups were mainly based on aircraft geometry, form factor, and weight. Using flat plate drag coefficients of various generic shapes, the drag at cruise velocity can be calculated at various store counts to estimate power necessary to operate at M3. This information creates an initial approximation for battery size based on energy consumption during various cruise conditions. This iterative process continually refines total aircraft weight and drag to converge on an optimized aircraft size and payload capacity.

4.3 Sizing and Design Trades

4.3.1 Aerodynamic Trade-Offs

Airfoil:

The two main consideration for the main wing airfoil section was CL_max and section drag at the cruise CL. For takeoff, the predicted Reynolds number range of 120,000 to 200,000 was used to compare CL_max of each airfoil. During the cruise segment of M3, the section drag was the primary consideration

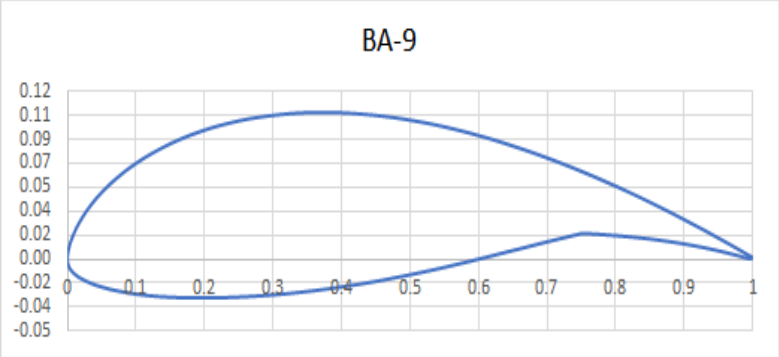

in evaluating airfoil performance. Assuming a velocity of 65 ft/s corresponding to 10-12 stores, the cruise Reynolds number range was predicted to be Re = 350,000 to Re = 420,000, and this range was used to compare the drag of each airfoil at a design cruise CL. The Reynolds number used to compare these airfoils lies in the 300,000 range. To narrow down the selection process, three airfoils were chosen which have the desired characteristics at low Reynolds numbers. The desired characteristics include a high CL max for takeoff and a low drag coefficient at low angles of attack for maximum cruise speed. The airfoils are shown below.

Figure 4.3: BA-9 Airfoil

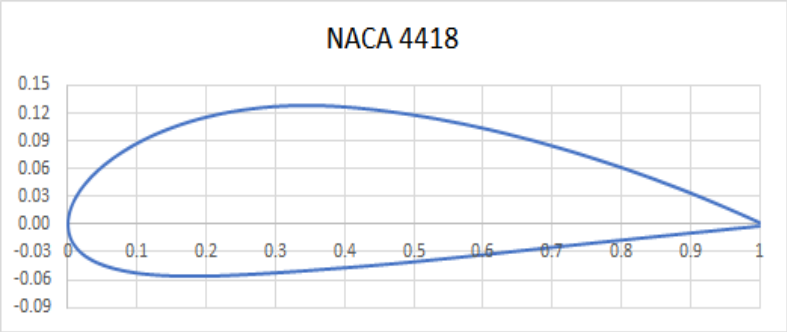

Figure 4.4: NACA 4418 Airfoil

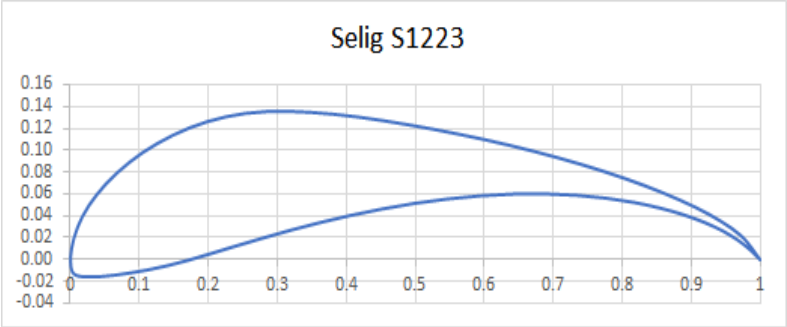

Figure 4.5: Selig S1223 Airfoil

Table 4.2: Characteristics of the NACA 4418, BA-9, and Selig S1223 Airfoils

	NACA 4418	BA-9	Selig S1223
Clmax at Re=200,000	1.53	1.54	2.29
Max t/c	18%	13.3%	12.1%
CD at Cl-.5 at Re= 400,000	.0098	.0088	.0363

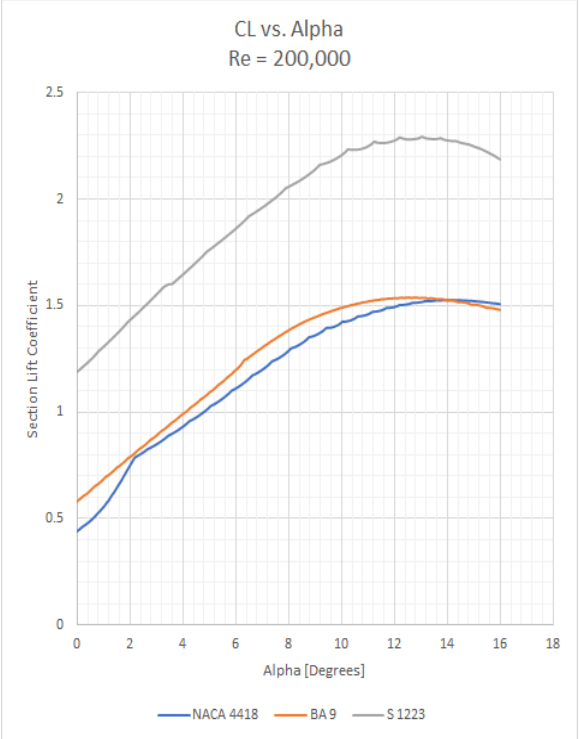

Figure 4.7: CL vs CD for High Reynolds Number

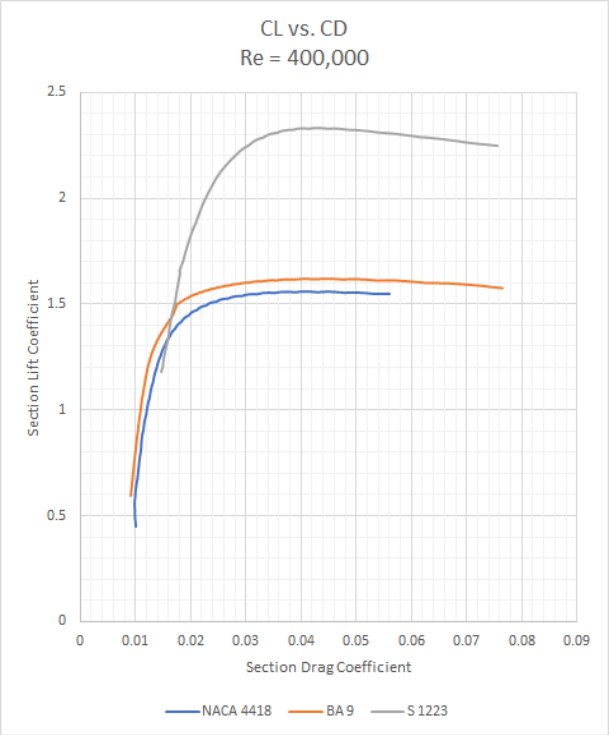

Figure 4.6: Graph of CL vs. Alpha for low Reynolds Number

CLmax was the driving criteria for airfoil selection because the takeoff constraint was a major driving factor. The Selig airfoil (S1223), designed for low Reynolds numbers (<200,000), has a significantly higher CLmax than other airfoils considered. For this airfoil, however, the geometry in the aft region was difficult to manufacture with precision and structurally challenging to accommodate control surfaces and surface actuators. Additionally, the airfoil thickness made wing structure more difficult to design and the low interior volume introduced significant challenges for integrating wing folding and locking actuators. The large interior volume and maximum thickness of the NACA 4418 was desirable to house wing folding and locking actuators, while its relatively flat bottom of the airfoil aided in the addition of the store mount and release mechanisms. The BA-9 airfoil section has higher CLmax and lower cruise section drag than the NACA 4418, but the thickness and outer mold line shape was less favorable when compared with the NACA 4418. Ultimately the NACA 4418 was chosen. The addition of flaps was analyzed to increase the CLmax for takeoff which is discussed more in detail in section [4].

Span:

To simplify the structure and integration of the wing folding and locking mechanism the number of folds in the wing had to be minimized. Multiple wing folds would create interference issues with externally mounted store mechanisms. Control surfaces would have to be divided and separated requiring additional actuators. Finally, the addition of extra folds complicates the structure of the wing and results in poor load distribution along the spar. A 6-foot wingspan could be comfortably folded within the 3’ stowed

configuration by dividing the wing into one 3’ main section and two 1.5’ wingtip sections. By angling the wingtips upward in its stowed configuration to 60 degrees, the span could be further lengthened to 6.25 feet, while the actuator force required could be halved.

Chord:

Short takeoff requirements pushed for a larger wing area to minimize takeoff thrust which would reduce power needed along with the total weight of the aircraft. During flight, however, a larger chord and smaller aspect ratio would potentially increase induced drag and power needed during operation. In addition, a heavier wingtip of larger chord would complicate load paths and require more structure for the folding and locking mechanism. Since span was fixed to 6.25 ft^2, chord had to be varied to achieve the appropriate wing area. The finalized chord length was chosen to be 12 inches to reduce wing loading while keeping Reynolds number high and weight low.

4.3.2 Propulsion Trade-Offs

Motor:

A motor capable of over 1600-W was required to achieve adequate takeoff performance. A preliminary analysis based around Newton’s Second Law created a simplified relation between thrust and takeoff weight. A 9-pound aircraft was calculated to require 12 pounds of static thrust to accelerate to takeoff. Additional factors such as vectored thrust and wheel friction were accounted for in a MATLAB takeoff code along with data from empirical flight tests. This relation between aircraft weight and thrust required allowed motors parameters to be bounded.

To maintain energy efficiency, high kV motors were analyzed to spin a large diameter propeller. Gearboxes and small in runner motors were initially considered to save weight compared to a larger outboard motor. Specific power comparisons, however, were not compelling enough to justify the extra cost and mounting complexities of a geared motor system.

Motor	kV (RPM/V)	Weight (oz)	Max Power (W)	Max Voltage (V)	Specific Power (W/oz)
Sunny Skies: X4120-8	465KV	10.86 oz	2000 W	18.5 V	184.16 W/oz
Sunny Skies: X4130-9	275KV	14.64 oz	2040 W	29.6 V	139.34 W/oz
Neumotor: 1710/1.5Y	650 KV	9.95 oz	1600 W	47.0 V	160 W/oz

Table 4.3: Motor Specifications

Ultimately, the Sunny Skies X4130-9 brushless outboard motor was selected. Static thrust tests with various propeller diameters and pitch combinations revealed the motor consistently produced the greatest amount of thrust for a given power input.

Propeller:

The main challenge in propeller selection is balancing the need for high static thrust on takeoff, and energy efficiency during flight. The high cruise speeds of M2 and M3 push for a propeller with high pitch as power decreases with velocity. The short field length, however, requires a large amount of static thrust in which a propeller with a high pitch would not be efficient or even provide the amount of thrust needed. Stowed configuration constraints along with adequate ground clearance limited the diameter of the propeller blades. Ultimately though static and flight tests, it was determined that a 19 x 8 propeller offered the ideal compromise between takeoff and operational performance.

Battery Selection:

Multiple battery cells were evaluated on their performance during M3, which involves takeoff at maximum gross weight and cruise at a high velocity. The estimated 1300 watts of power required for takeoff set the battery discharge criteria, while the predicted 500 watts of cruise power dictated the battery energy requirements.

Battery	Weight (oz):	Energy Density: kJ/oz	Empirical Efficiency:	Empirical Discharge Rate: 1/Hr
Elite 1500	.86	7.53	85%	15
Elite 5000	2.4	9.00	60%	10
Tenergy 1600	.87	7.94	30%	5

Table 4.4: Battery Specifications

Batteries were evaluated based on their energy density, discharge rate, and charge efficiency to meet the range and power required. Selection goals were based around minimizing the weight of the flight packs while maintaining the required capacity and discharge rates. Performance tests were conducted with a battery analyzer to construct discharge curves representative of missions M2 and M3. In addition, tests were also conducted with high loads to evaluate the battery's maximum current output.

The Elite 1500 batteries were chosen for their superior charge efficiency and high discharge rate. The Elite 5000 and Tenergy 1600 cells have a higher theoretical energy density but empirical discharge tests revealed a much lower utilization of their capacity, with the Tenergy cells utilizing as little as a third of their energy capacity. Additionally, both cells had far lower discharge rates which resulted in less thrust during periods of peak power. Overall the Elite 1500 battery cells consistently provided more power and discharged a higher percentage of their capacity during various performance tests compared to other battery cells.

4.3.3 Final Optimized Aircraft

Through testing a careful consideration, the following design choices were made for the aircraft: The wings for final optimized aircraft utilizes the NACA 4418 airfoil, with a span of 6.25 feet and a chord of 12 inches. The propulsion system consists of the Sunny Skies X4130-9 brushless outboard motor, a 19 x 8 propeller, and Elite 1500 battery cells.

4.4 Lift Drag and Stability Characteristics

Lift over drag is plotted against airspeed for the empty aircraft for all three mission profiles. Missions 2 and 3 operate at much lower L/D as compared to Mission 1 because the higher mission velocities increase the effects of parasitic drag. This is further illustrated by the drag breakdown of each major aircraft component. Drag from the exposed payload stores and mounts require a significant amount of power to overcome.

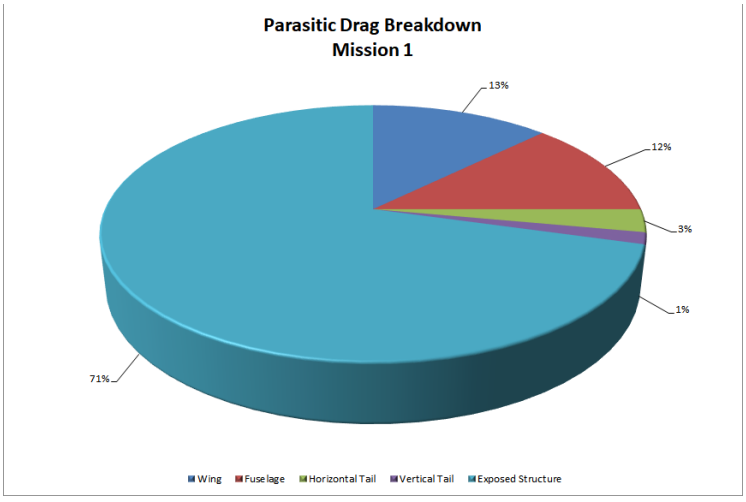

Figure 4.8: Parasitic Drag Breakdown for Mission 1

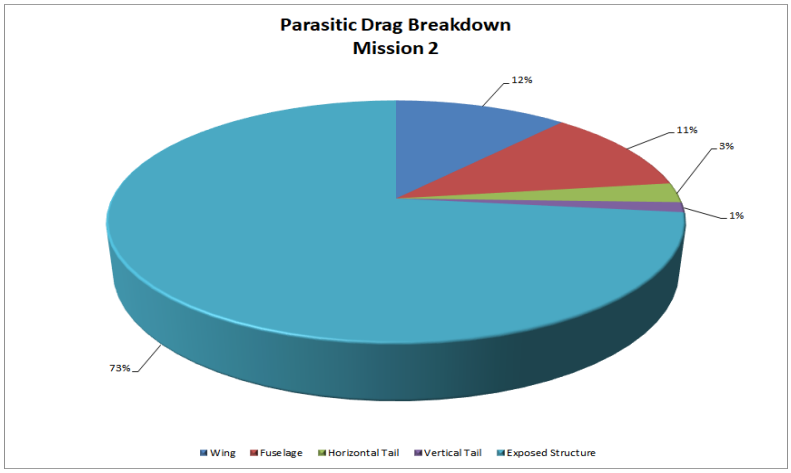

Figure 4.9: Parasitic Drag Breakdown for Mission 2

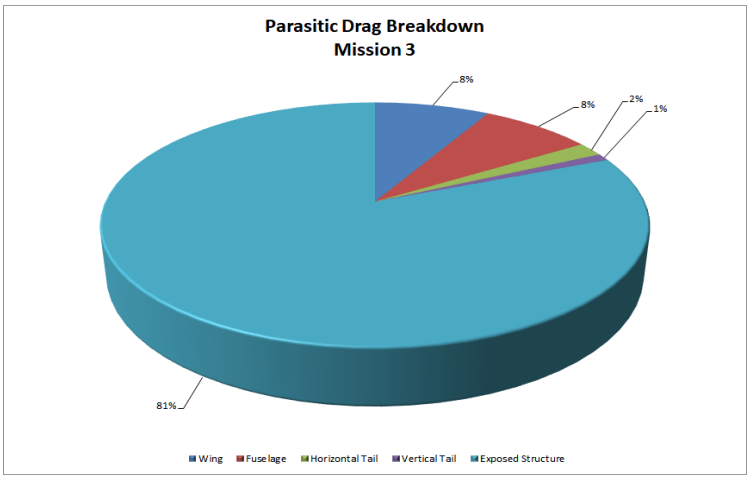

Figure 4.10: Parasitic Drag Breakdown for Mission 3

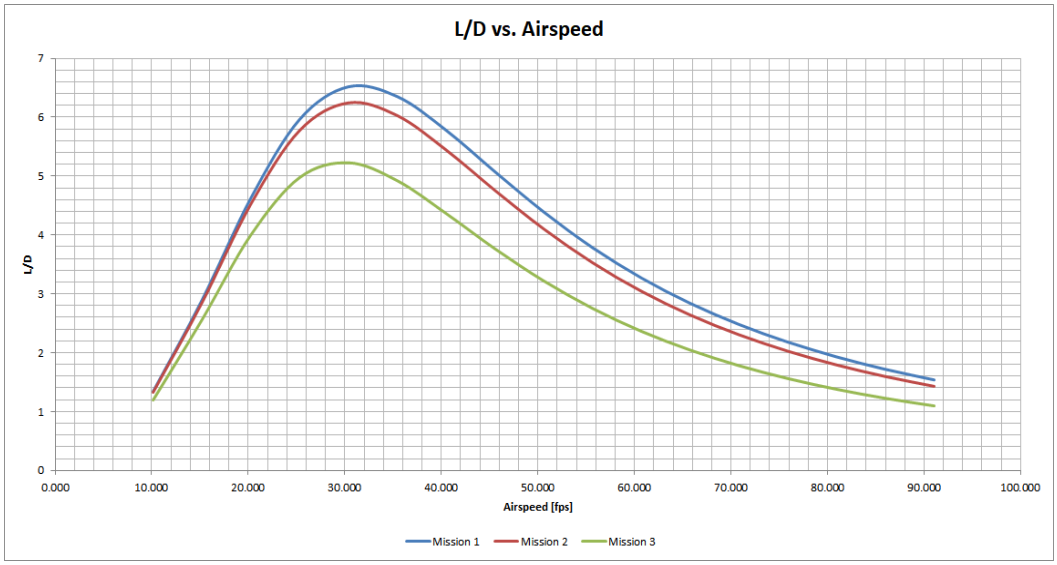

Figure 4.11: L/D vs. Airspeed for Missions 1, 2, and 3

4.4.1 Stability and Control

Athena Vortex Lattice (AVL) is used as preliminary analysis tool to evaluate the span loads for preliminary structural sizing, neutral point for CG location, preliminary estimations for stability and control of the aircraft. Primary considerations were based around analyzing takeoff characteristics. The short field length of the runway meant that adequate rotation was an important facet to a successful takeoff. Care was taken to reduce the static margins with confidence to be able to sufficiently rotate upon takeoff. Additional points of analysis was the effectiveness of flaperons and its effects on stability during takeoff regarding various lengths and degrees of deflection.

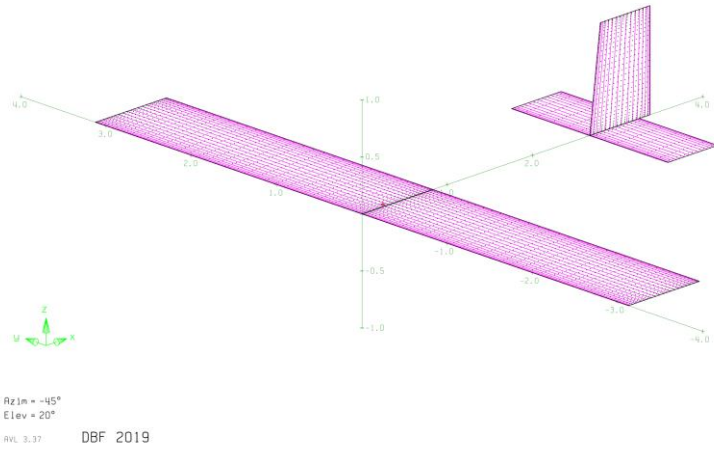

Figure 4.12: AVL input geometry

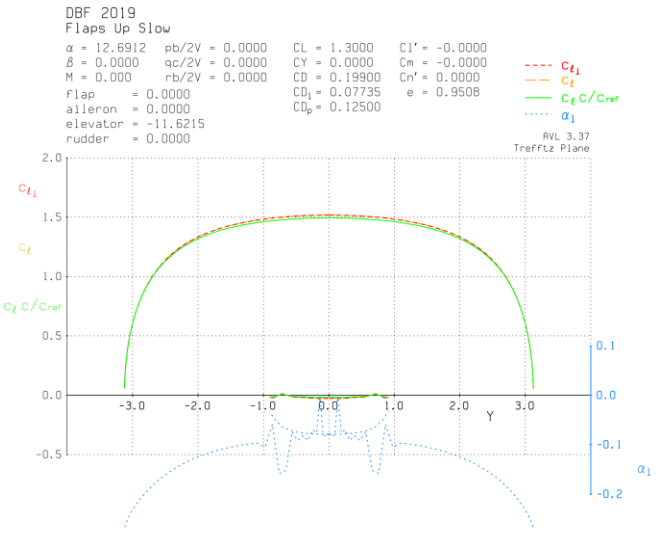

Figure 4.13: AVL Treffz Plot

All modes achieve level one criteria for a class I plane per MIL-SPEC 8785C [1] with two exceptions. The only unstable mode was the spiral with a slight divergence. The spiral mode is, in fact, worse than level 3, with a time to double of 1.95 seconds. Flight testing showed that this deficiency was not obtrusive to the pilot. Furthermore, this deficiency is for slow flight with flaps down. This flight condition is experienced only for a brief time during takeoff. The time to double is closer to 5 seconds, which is the level 3 threshold, for slow flight with flaps up. This flight condition is the beginning of the climb segment, and the aircraft is only in this flight condition for a brief time duration. During cruise, the spiral mode is near level 2, with a longer time to double. The lack of dihedral is the likely cause for this deficiency. In addition, the Control Anticipation Parameter satisfies the level two handling qualities criteria, having an η/α of 6.62 G's/rad with a short period natural frequency of 6.77 rad/sec. As discussed by Cook [2], level two handling qualities are stated as, 'Flying qualities adequate to accomplish the mission flight phase, but with an increase in pilot workload,' thus not requiring augmentation for mission performance. Upon conducting further research, it was found that the recommendations in MIL-SPEC 8785C are applicable to small-scale Unmanned Aerial Vehicles (UAVs) as discussed by Tyler Foster of Brigham Young University [3].

A Trefftz plane, shown in Figure 4.13, was created with the geometry input in Figure 4.12. This plot verified that the peak CL occurred within 50% of the semi-span and that at any section, specifically the wingtips, CL's did not exceed CL max. AVL takes the input geometry and uses an extended vortex lattice method to calculate the aerodynamic performance as well as the stability and control derivatives. Figure 4.13 shows the resulting pole-zero map of the eigenvalues calculated by the program.

4.5 Predicted Mission Performance

Mission 1		
Flight Conditions (Empty)		
Cruise Airspeed (ft/s)	45	
Wind Speed (ft/s)	0	
Climb Rate (ft/min)	600	
Turn G-loading (g)	1.41	
Flight Segment	*Time (s)*	Power (J)
Take Off	1.25	1500
Climb	11.11	5550
180 Degree Turn	5.55	2220
500 ft Downwind	11.11	4444
360 Degree Turn	11.11	4444
500 ft Downwind	11.11	4444
180 Degree Turn	11.11	4444
1000 ft Upwind	22.22	8888
2 More Laps	133.33	57768
Landing Segment	33.33	13332
Total/Max/Total	251.23	93702
Max Available	300	320400
Margin [%]	16%	71%

Table 4.7: Mission 1 Performance Prediction

Mission 2	
Flight Conditions (Radome, no stores)	
Cruise Airspeed (ft/s)	80
Wind Speed (ft/s)	0

Climb Rate (ft/min)	1200	
Turn G-loading (g)	2	
Flight Segment	*Time (s)*	Power (J)
Take Off	1.25	1500
Climb	7.14	8400
180 Degree Turn	4.51	4961
500 ft Downwind	6.25	6875
360 Degree Turn	9.03	9933
500 ft Downwind	6.25	6875
180 Degree Turn	4.51	4961
1000 ft Upwind	12.50	13750
2 More Laps	85.00	94710
Landing Segment	33.33	13332
Total/Max/Total	169.77	165297
Max Available	300	320400
Margin [%]	43%	48%

Table 4.8: Mission 2 Performance Prediction

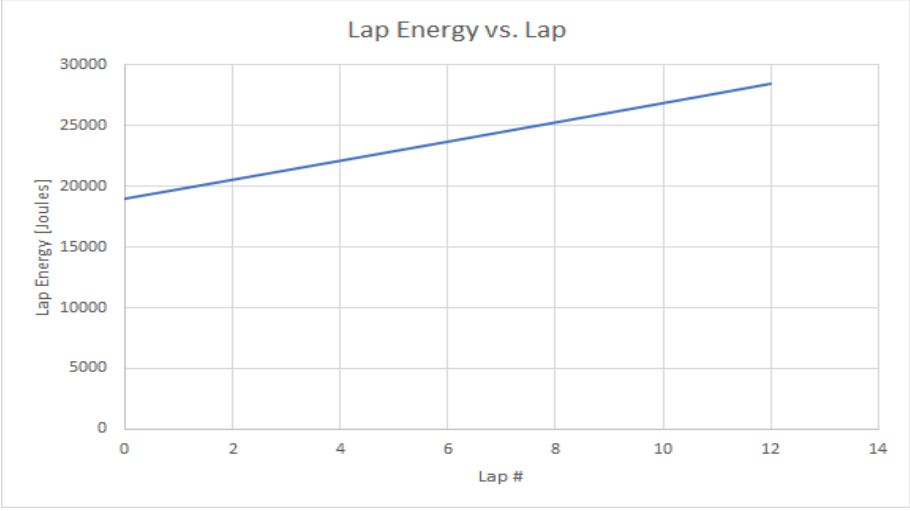

Figure 4.14: Lap Energy vs. Lap Number

5.0 Detail Design

After optimizing the dimensions of the aircraft, a prototype was manufactured and tested to verify the mission profile predictions.

5.1 Design Parameters

5.1 Design Parameters:			
Wing		**Motor**	
Span	75	**Band/ Model**	Sunny Skies: X4130-9
MAC	12	**Effective kV**	275KV
Aspect Ratio	6.25	**Max RPM**	8000
Wing Area (ft^2)	6.25	**No Load Current**	1.6 A
Airfoil	NACA 4416	**Winding Resistance ()**	33 mOhm
		Peak Power	2040 Watts
Aileron		**Propeller**	19 x 8
Span		**Propulsion Battery:**	
Chord % of wing		**Cell Type**	Elite 1500 NiMH
Deflection		**Cell Capacity (aH)**	1.5 aH
Horizontal Tail		**Number of Cells**	84
Span (ft)	2.3	**Nominal Voltage**	1.2
Chord	8 in	**Maximum Current (A)**	70
Area (ft^2)	1.6	**Internal resistance (mOhm)**	12
Airfoil	NACA 0014	**Flight Control System**	
Vertical Tail		**Speed Controller**	Phoenix Edge Lite HV 80Amp
Span (ft)	1.2	**Flight Radio**	Futaba T-14 SG
Chord (in)	8	**Flight Receiver**	Futaba R7008SB 8+
Area (ft^2)	0.8	**Servomotor #**	5

Airfoil	NACA 0014	**Servomotor**	HiTec HS-5065MG
Total tail weight	3 (h) 2(v) 5 oz (total)		

Table 5.1: Design Parameters

5.2 Structural Characteristics

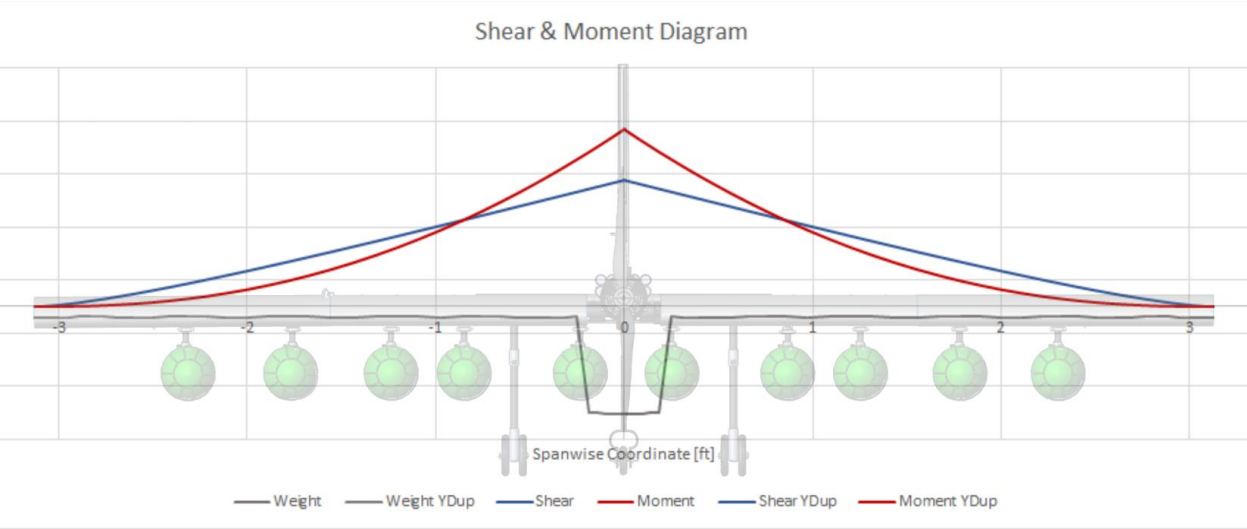

Figure 5.1: Shear and Moment Diagram

Before a formal detailed design could be finalized, an analysis of the loads along the wing and fuselage were made in both flight and landing scenarios. The wing folding requirement complicated load paths and requires a comprehensive analysis of stresses carried by the wing during flight. Figure 5.1 shows the shear and moment diagram for the maximum aircraft weight. All loads during takeoff and landing transmit from the landing gear through the spar and to the boom. This design loads the strongest members of the aircraft and avoids having structural parts. Coupled with the lightweight wing and tails, all major components combine to make a lightweight aircraft that can effectively compete for the highest score.

5.3 System Design and Component Selection/Integration

The following subsystem components were analyzed with more detail to finalize the aircraft design.

5.3.1 Wings

A build up balsa design was selected because of its lightweight structure that gives control over internal space. Balsa ribs could be cut to mount and accept wing folding and locking actuators which

facilitated integration. Strategically spaced longerons created points to anchor store drop mechanisms and actuators.

Load paths were an important consideration around the two wing joints. Moments and shear stresses carried through each joint which meant that the folding and locking joints must be effectively anchored to the spar. For this reason, a thin walled, pultruded carbon fiber rod was chosen as the main spar. A balsa and composite spar would be slightly lighter because structure can be lightened as spar loading decreases across the span. A carbon fiber spar, however, provided a more durable surface which locking mechanisms could be fixed with adhesive. Additionally, the carbon fiber tube was durable enough for structures, such as the landing gear, to transfer forces directly the into spar, reducing the portions of the wing that needed to bear load. This resulted in a simpler wing design with more room to house folding and locking components and store mechanisms.

5.3.2 Folding Mechanism

Initially, worm gears were considered as a folding mechanism because of their ability to apply mechanical advantage and their inability to be driven backwards, thus acting as an added safety measure to keep the wings folded down. Additionally, one servo motor could be geared to drive two worm gears on either side of the wing. The high gear ratio of most worm gears, however, meant that a large number of rotations from the actuators were required to rotate the hinge 270 degrees. Servo motors capable of rotations above 180 degrees were either exceedingly large or could not have stops programmed to halt operation.

Instead, a design incorporating linear actuators and pulleys was selected. Small and lightweight linear actuators were found (Actuonix L-16) which had a stroke length of 140mm.

The wings were folded around plastic hinges built onto 3D printed end ribs affixed to each side of the wing joint. Two ⅜ inch pulleys were glued onto the end ribs, concentric to the hinge pin. Folding was accomplished by a linear actuator (Actuonix L-16) pulling a cable anchored to the end of one pulley. The pulley, endplate, and wingtip rotate around hinge pins from a stowed to its deployed position.

The second pulley has another cable anchored in such a way that it is in tension once the wingtip folds past 90 degrees. It is also anchored to the linear actuator to prevent the wingtip from slamming down into its folded position.

Figure 5.2: Wing folding hinge

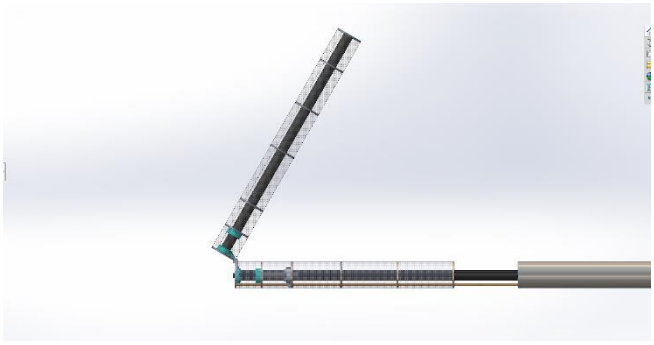

Figure 5.3: Wing Folding

Due to its resistance to stretch and ability to be easily crimped into position while avoiding the formation of knots inside the wing, ⅛ inch stainless steel cable was selected. The maximum pull force of the L-16 linear actuators is 17lbs. Through a force balance, it was found that unfolding the wingtips from a stowed angle of 60 degrees halved the amount of force required compared to wingtips stowed at 0 degrees, lying flat on the main section.

5.3.3 Locking Mechanism

Carbon fiber pins were mounted parallel to the spar with 3D printed rails on the main section of the wing. Each pair of locking pins was affixed on a carriage such that they slide together. On the wingtip portion, a pair of carbon fiber ferrules were mounted such that they corresponded to the spacing and position of the locking pins. The wingtip locks by sliding the pins into their corresponding ferrules using a linear actuator (Actuonix L-12). In this position the wingtip spar is concentric to the main spar and the surface of the wing is aligned.

The pins are sized such that 3 inches of pin engage each ferrule to allow an adequate length of tube to brace the wing joint. The use of 2 tubes and rails transfer stress, bending, and torsional loads from the wingtip to the main section spar.

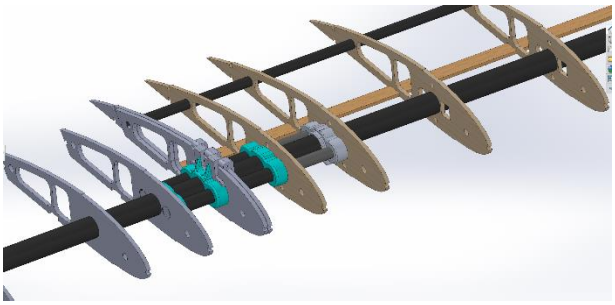

Figure 5.4: Wing Locking configuration

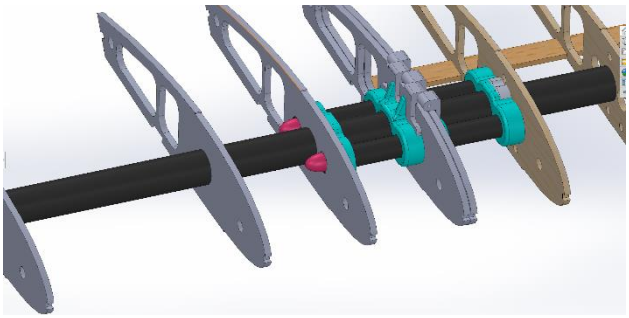

Figure 5.4: Wing Locking configuration

5.3.4 Store Drop Mechanism

Weight, drag, and reliability were the primary factors considered in the design and development of our store drop mechanisms. The mission 3 specifications indicate that stores, which must be carried externally (the first four under the wing), dropped once per completed lap will be added to the overall mission 3 score.

Prior to the release of “DBF Q&A #1,” it was believed that no microcontroller or additional transmitter would be allowed in this year’s competition – which heavily influenced early designs. To minimize the number of servos necessary to actuate individual stores, early concepts included a single servo pulling a carbon rod with attached hooks that would release the restraining mechanism. However, after the release of the first Q&A form, it was decided that having a small, programmable servo motor

(Hitec HS-40's) for each release mechanism would make the system more reliable. These servo motors are actuated through the controls of a separate remote transmitter.

Because of the stores' unique shape and weight distribution, a two-component restraint system was chosen to securely carry the airplane's payload. One component of this system, the front ring, was chosen for its low drag and light weight. To support the middle and rear sections of the stores, a second component, the mechanism itself, was placed at the end of the store's football-shaped front to prevent unnecessary movement. While some early mechanism designs proved to be very lightweight and small (notably a single hook design), most did not reliably restrain the stores in flight. To combat this issue, a parallel link claw grip design was implemented. Controlled by a single servo, each mechanism releases the store as the claw grip opens. These mechanisms are made of 3D-printed components, carbon tubing, and small pins.

Figure 5.6: Store drop mechanism

5.3.5 Tail Hook

Weight, manufacturability, and ergonomics were primary factors when selecting the material and form of the tail hook design. Regarding ergonomics, the ground crew must be able to restrain the aircraft without undue burden and be able to release the aircraft, at the pilot's command, consistently. This was a major consideration in the shape, length, material, and interface (for the ground crew) of the tail hook. Experimenting with an estimated load of 15 lbs. generated by the front propeller, it became clear that a simple knot or loop clamped by metal sleeves – which is easy to manufacture – for the ground crew's finger would not only be functional but would cause little discomfort. Testing of different materials (metal wire, string, Kevlar tow) showed that all materials would withstand the force of the propeller beyond a factor of safety of 2.

Tail Hook Material Selection			
Material	**Weight (oz/ft)**	**15 (lb) Test**	**30 (lb) Test**
Metal Wire	.065	Pass	Pass
Kevlar String	.017	Pass	Pass
Kevlar Tow	.003	Pass	Pass

Table 5.2: Tail Hook Material Properties

5.3.6 Radome

The considerations for the cross-section of the disk were drag, lift, and moment. While it is important to reduce drag of the radome disk and pylon for mission 2, it is also important to reduce lift and moment, in the operational envelope of the aircraft, so that the disk, pylon, and attachment structure does not endure significant loads. This consideration also extends to the stability and control of the aircraft, which is discussed in more detail in “Stability and control’’. Hoerner states that for, for small angles of attack, cross-section with sharp leading edges have significant ability to produce lift. For us, this is undesirable. Hoerner suggests that an approximately elliptical cross-section has a low ability to produce lift, which is desirable for this application so that structure and actuator size can be reduced [3]. Since a spherical radome is impractical, we opted to create a radome with an elliptical cross section.

The detachable base is two parts and streamlined to the radome with a tube that fits into a streamlined base attached to the main boom. Within the streamlined base attached to the main boom, a splined axle transfers the rotation form a continuous servo to the radome.

The size and cross-section of the radome was a major consideration in the design. Minimum size requirements for the diameter and thickness, at the center, are a competition external requirement. The rules also state the that radome operation must be visible from the ground. The size and color scheme enhance this. Using inspiration from the Air Force/Navy aircraft radome for the paint scheme, earlier testing proved the disk operation was visible from the ground with a 12-inch disk and a single stripe of a contrasting color to the base coat color.

The considerations for the cross-section of the disk were drag, lift, and moment. While it is important to reduce drag of the radome disk and pylon for mission 2, it is also important to reduce lift and moment, in the operational envelope of the aircraft, so that the disk, pylon, and attachment structure does not endure significant loads. This consideration also extends to the stability and control of the aircraft, which is discussed in more detail in Section 4.4.1. Referencing Hoerner [4], for small angles of attack, cross-section with sharp leading edges have significant ability to produce lift. For us, this is undesirable. Hoerner suggests that an approximately elliptical cross-section has a low ability to produce lift, which is desirable for this application so that structure and actuator size can be reduced.

5.3.7 Fuselage Boom

The central carbon fiber boom is the main structural member connecting the entire aircraft. The motor, battery, wings, fuselage, and empennages are all connected to this boom.

5.3.8 Motor Mount

The motor mount is 3D printed and affixed to the end of the fuselage boom. The motor bolts directly to the mount.

5.3.9 Electronic Speed Control

ESC	Max Continuous Current (A)	Max Voltage	Weight (oz)
HobbyWing Flyfun ESC 100A High Voltage	100	50	3.95
PHOENIX EDGE HV 80 AMP ESC	80	50.4	4.40
PHOENIX EDGE LITE HV 80 AMP ESC	80	50.4	3.03

Table 5.3: Electronic Speed Controls Specifications

With a peak power of 1600 Watts and high nominal voltage of 33.6 volts, many high voltage Electronic Speed Controls (ESC) were tested. It was found the Phoenix Edge Lite High Voltage esc was the lightest option that was able to safely handle the necessary power with sufficient cooling.

5.3.10 Control Surface

The size of the control surfaces on the main wing were governed by the interior wing structure and the location of the wing folding hinge. For the ailerons, the control surface was confined to the outer tip to simplify the installation and actuation. The aft structural spar in the main wing is located at approximate 0.8C so the aileron and flap control surface chords are 0.2C. From AVL analysis and flight testing, the pilot had adequate control on at low speeds. During takeoff, the flaps are set 25 degrees down and the ailerons are drooped 20 degrees. The ailerons are flaperon control surfaces during the takeoff segment. This improved the CLmax by 20% and, since roll control was reduced slightly, this decrease was unobtrusive to the pilot. The control surfaces for the horizontal and vertical tail surfaces are 0.25C. This provided adequate pitch and yaw control, especially during the demanding takeoff segment. The hinge moments were predicted from vortex lattice methods to ensure that the geometry did not require unintentionally large control actuators.

To maintain the airfoil shape and the aerodynamic properties of the airfoil, they must be manufactured as close to the airfoil shape as possible. A foam-fiberglass composite is chosen over a balsa structure because it is similar in weight, provides more torsional stiffness, and can be consistently manufactured.

5.3.11 Servo Selection:

By analyzing the hinge moments from each surface using AVL, the Hitec HS5065 MG

servo was chosen because it has enough torque to move both the rudder and ailerons which required a calculate 16 oz/in of torque. With a nominal 31 oz/in of torque the Hitec micro servo provide enough factor of safety while maintaining a compact and lightweight form factor.

5.3.12 Landing Gear

Two options were considered for the main gear of the tricycle configuration: two rigid struts anchored to the wing spars and an inverted U-shape anchored to the main boom. While the inverted U Shape is shock-absorbing and allows for some flexibility, it interfered with store spacing underneath the main fuselage. A V-shape configuration anchored onto the wing spars was selected since the wing spars are an ideal structural and load bearing member.

5.4 Weight and Balance

The aircraft is expected to weigh 10 lbs with an empty with a maximum weight of 12 lbs. Components are places such that the center of gravity (C.G.) falls between 23-28%. Below is a table of weights for missions 1-3. Moments are measured 30 inches ahead of the ¼ chord

	Component	**Arm (in)**	**Weight (oz)**	**Moment (oz * in)**
Structure	Motor Mount	19	0.03	0.57
	Boom	39.5	2.56	101.12
	Wings	30	30.56	916.80
	Empennage	63.75	5.12	326.40
Propulsion	Speed Controller	23	3.04	69.92
	Battery Pack	32.25	22.56	727.56
	Motor	17.5	14.64	256.20
	Propeller	16	2.60	41.60
Avionics	Receiver	23	0.40	9.2
	Receiver Battery Aileron Servos	25	2.10	52.50
	Horizontal Servo	30.5	0.77	23.49

	Vertical Servo	31	0.77	23.87
Landing Gear	Front Gear	22	0.40	8.80
	Main Gear	34.64	2.16	57.24
	Tail Hook	63.75	0.85	54.19
Payload	Store Actuator	30	0.06	1.80
Wing Actuator	Folding Actuator	30	2.29	68.70
	Lock Actuator	30	1.41	42.30
Radome	Radome	36.25	1.35	48.94
	Radome Mount	37	1.40	51.80

Table 5.4: Weight and Balance of Aircraft

Mission 1	**Component**	**Arm (in)**	**Weight (oz)**	**Moment (oz * in)**
Aircraft	Empty Aircraft			
	Battery	32.25	67.68	2182.68

Table 5.5: Weight Breakdown of Aircraft for Mission 1

Mission 2	**Component**	**Arm (in)**	**Weight (oz)**	**Moment (oz * in)**
Aircraft	Empty Aircraft			
	Battery	32.25	67.68	2182.68
Payload	Radome & Mount	36.75	2.8	102.9

Table 5.6: Weight Breakdown of Aircraft for Mission 2

Mission 3	**Component**	**Arm (in)**	**Weight (oz)**	**Moment (oz * in)**
Aircraft	Empty Aircraft			
	Battery	32.25	67.68	2182.68
Payload	Stores	30	13	390

Table 5.7: Weight Breakdown of Aircraft for Mission 3

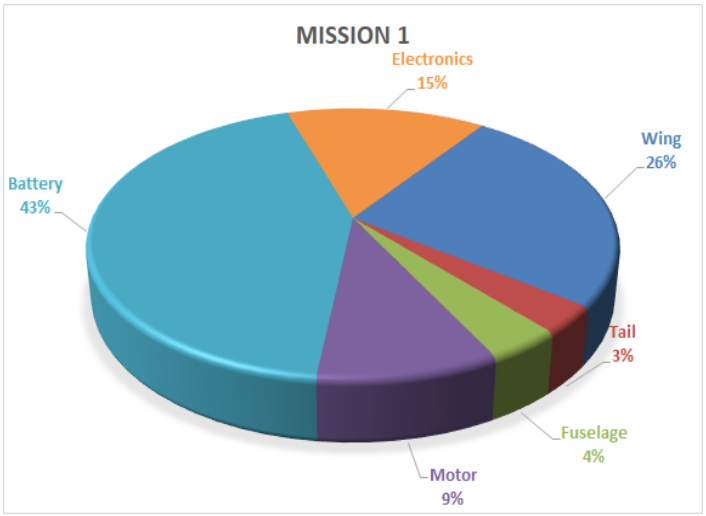

Figure 5.7: Visual Breakdown of Weight Percentages for Mission 1

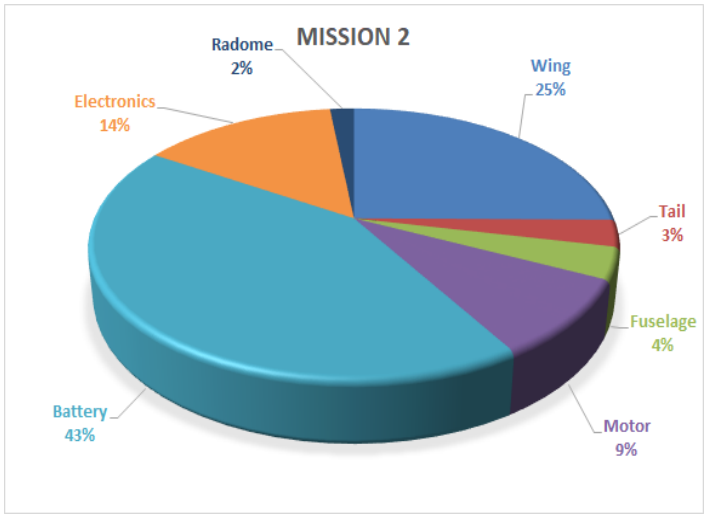

Figure 5.8: Visual Breakdown of Weight Percentages for Mission 2

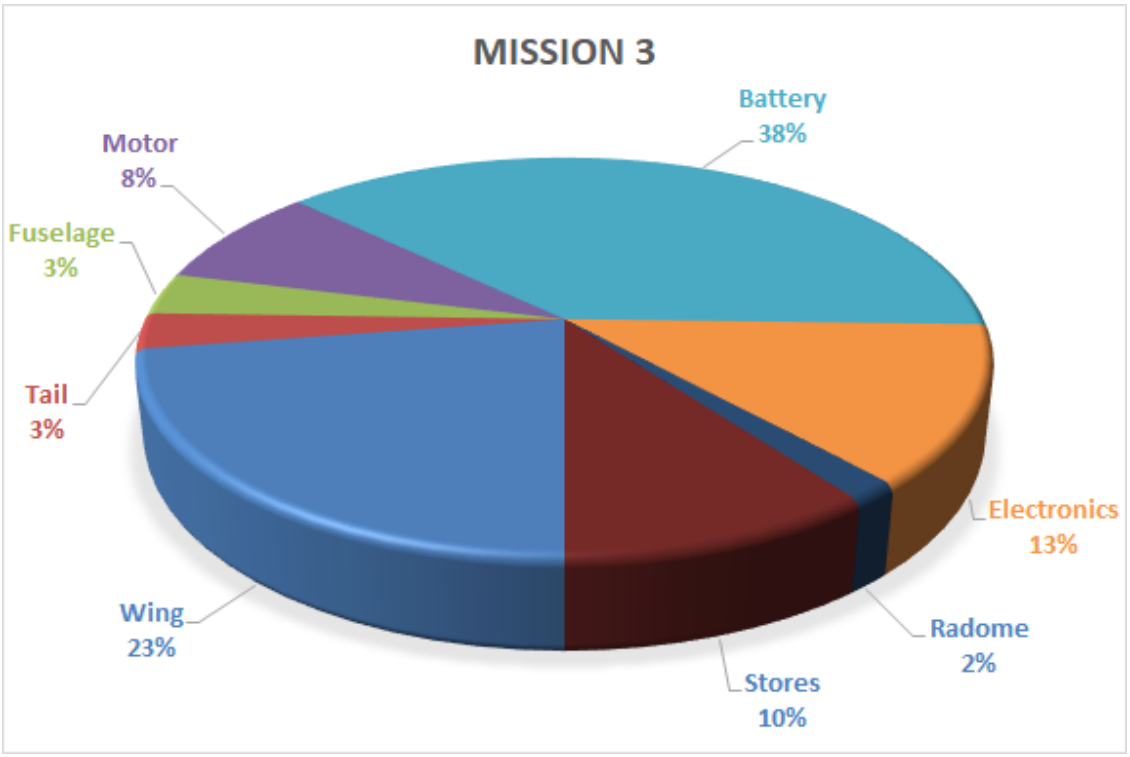

Figure 5.9: Visual Breakdown of Weight Percentages for Mission 3

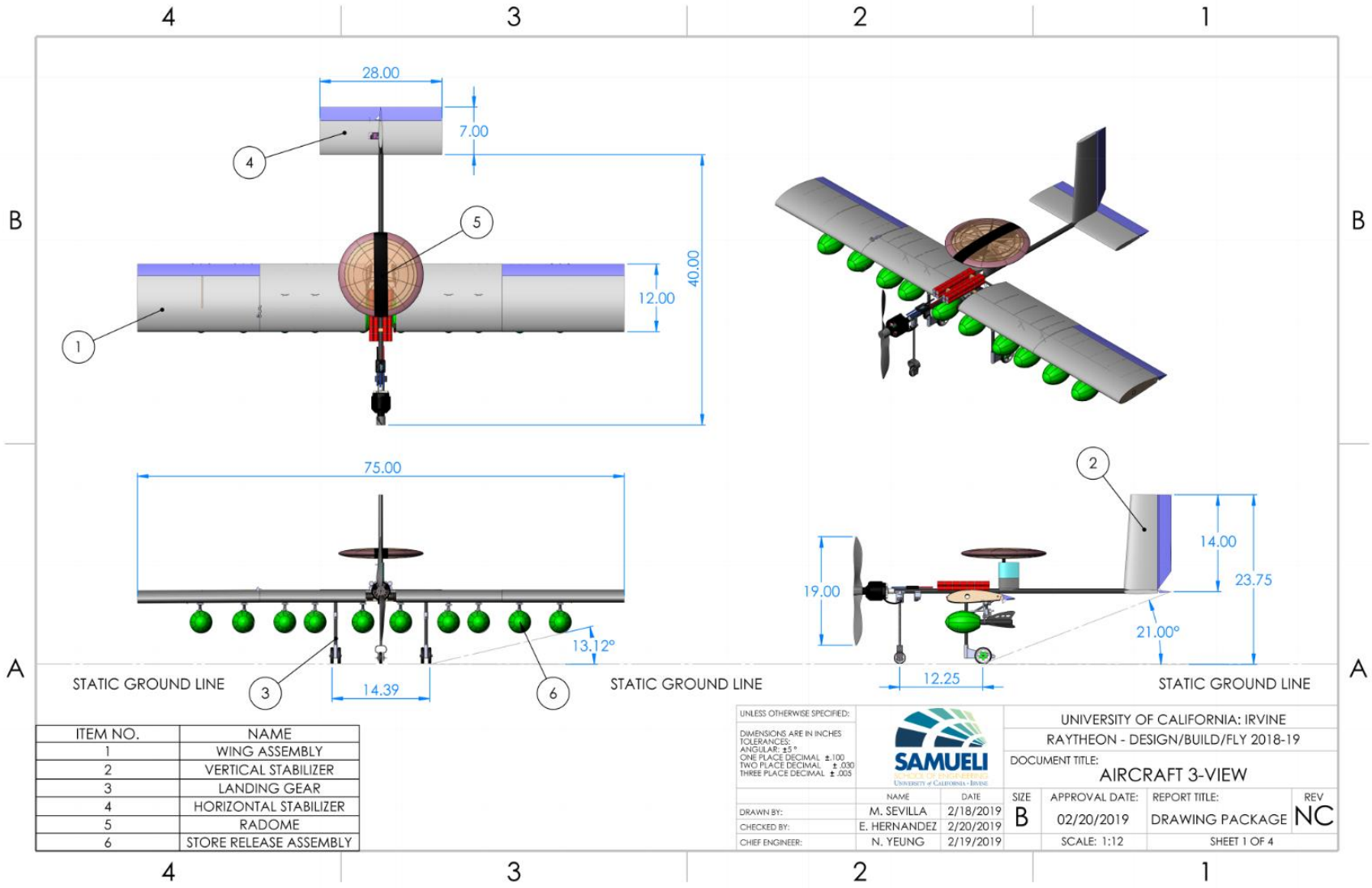

ITEM NO.	NAME
1	WING ASSEMBLY
2	VERTICAL STABILIZER
3	LANDING GEAR
4	HORIZONTAL STABILIZER
5	RADOME
6	STORE RELEASE ASSEMBLY

UNLESS OTHERWISE SPECIFIED:
DIMENSIONS ARE IN INCHES
TOLERANCES:
ANGULAR: ±5 °
ONE PLACE DECIMAL ±.100
TWO PLACE DECIMAL ±.030
THREE PLACE DECIMAL ±.005

SAMUELI SCHOOL OF ENGINEERING, UNIVERSITY of CALIFORNIA - IRVINE

UNIVERSITY OF CALIFORNIA: IRVINE
RAYTHEON - DESIGN/BUILD/FLY 2018-19
DOCUMENT TITLE:
AIRCRAFT 3-VIEW

	NAME	DATE
DRAWN BY:	M. SEVILLA	2/18/2019
CHECKED BY:	E. HERNANDEZ	2/20/2019
CHIEF ENGINEER:	N. YEUNG	2/19/2019

SIZE B | APPROVAL DATE: 02/20/2019 | REPORT TITLE: DRAWING PACKAGE | REV NC
SCALE: 1:12 | SHEET 1 OF 4

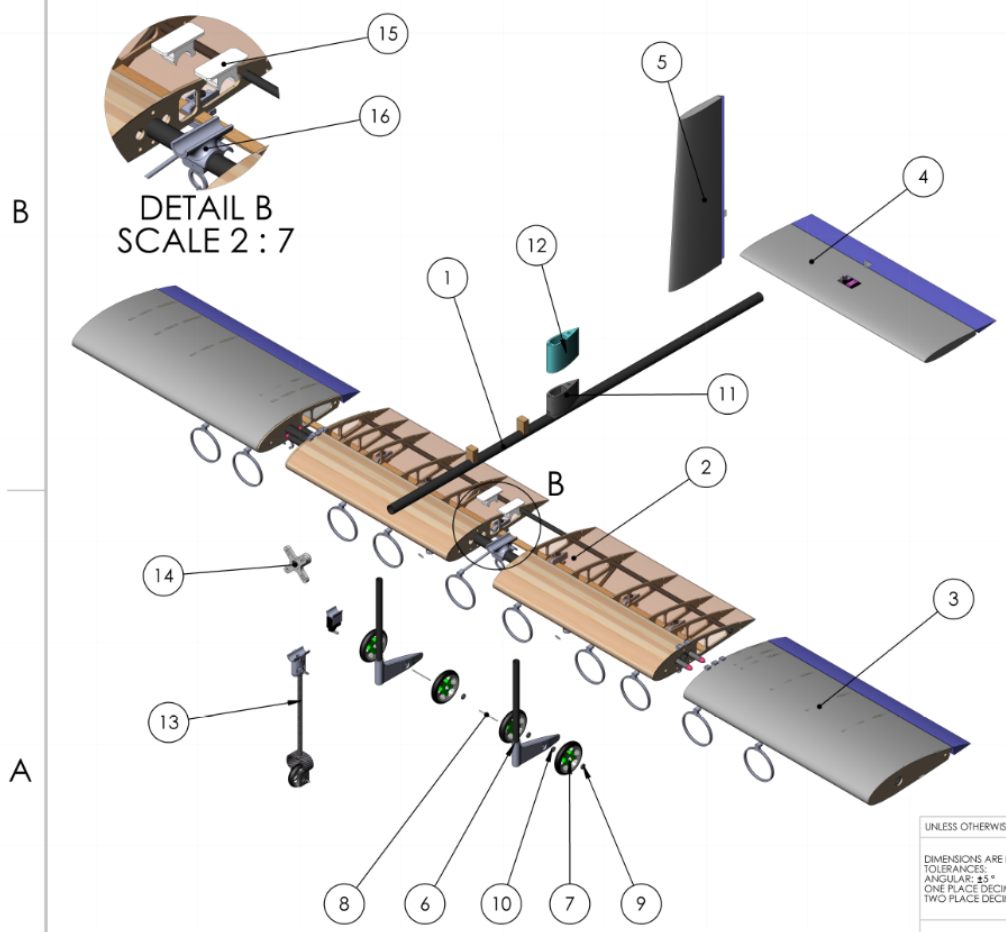

ITEM NO.	NAME	MATERIAL	QTY
1	BOOM	CARBON FIBER	1
2	CENTER WING ASSEMBLY	BALSA - MICROLITE	1
3	WING TIP ASSEMBLY	BALSA - MICROLITE	2
4	HORIZONTAL STABILIZER	FOAM - FIBERGLASS	1
5	VERTICAL STABILIZER	FOAM - FIBERGLASS	1
6	LANDING GEAR STRUT	CARBON FIBER - ABS PLASTIC	2
7	LANDING GEAR WHEEL	PLASTIC - RUBBER	3
8	LANDING GEAR AXLE (MAIN)	STEEL	2
9	LANDING GEAR WASHER	ABS PLASTIC	10
10	LANDING GEAR BEARINGS (MAIN)	PLASTIC - CERAMIC	4
11	RADOME SUPPORT STRUCTURE	ABS PLASTIC	1
12	LANDING GEAR STEERING STRUT	ABS PLASTIC - CARBON FIBER	1
13	FOWARD LANDING GEAR ASSEMBLY	CARBON FIBER	1
14	MOTOR MOUNT	ABS - PLASTIC	1
15	BATTERY MOUNT	ABS - PLASTIC	2
16	WING SPAR - BOOM MOUNT	ABS - PLASTIC	1

UNLESS OTHERWISE SPECIFIED:
DIMENSIONS ARE IN INCHES
TOLERANCES:
ANGULAR: ±5°
ONE PLACE DECIMAL ±.100
TWO PLACE DECIMAL ± .030

SAMUELI SCHOOL OF ENGINEERING
UNIVERSITY of CALIFORNIA • IRVINE

UNIVERSITY OF CALIFORNIA: IRVINE
RAYTHEON - DESIGN/BUILD/FLY 2018-19
DOCUMENT TITLE:
STRUCTURAL ARRANGEMENT

	NAME	DATE
DRAWN BY:	M. SEVILLA	2/19/2019
CHECKED BY:	E. HERNANDEZ	2/21/2019
CHIEF ENGINEER:	N. YEUNG	2/21/2019

SIZE	APPROVAL DATE:	REPORT TITLE:	REV
B	2/21/2019	DRAWING PACKAGE	NC
	SCALE: 1:7	SHEET 2 OF 2	

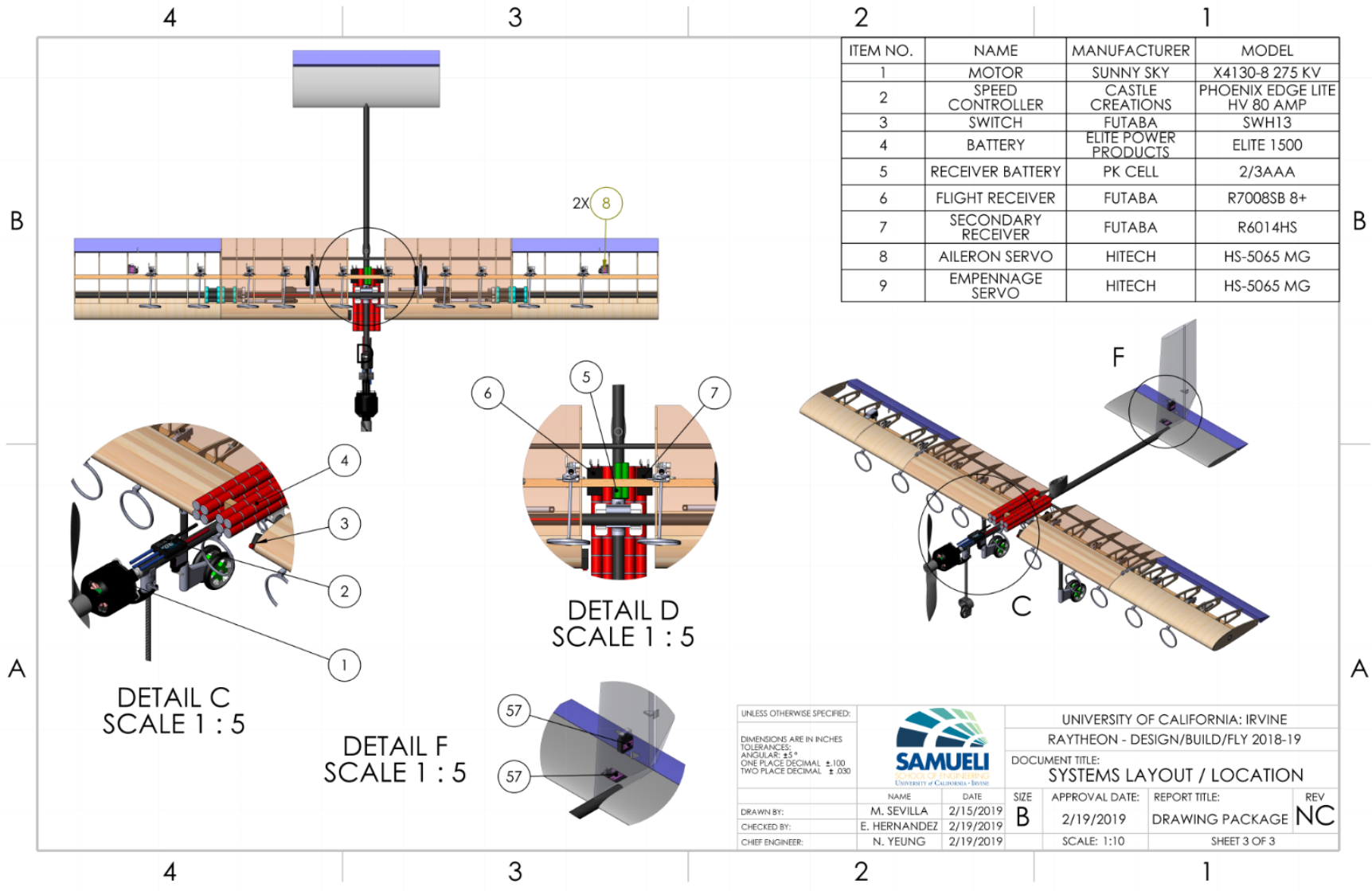

ITEM NO.	NAME	MANUFACTURER	MODEL
1	MOTOR	SUNNY SKY	X4130-8 275 KV
2	SPEED CONTROLLER	CASTLE CREATIONS	PHOENIX EDGE LITE HV 80 AMP
3	SWITCH	FUTABA	SWH13
4	BATTERY	ELITE POWER PRODUCTS	ELITE 1500
5	RECEIVER BATTERY	PK CELL	2/3AAA
6	FLIGHT RECEIVER	FUTABA	R7008SB 8+
7	SECONDARY RECEIVER	FUTABA	R6014HS
8	AILERON SERVO	HITECH	HS-5065 MG
9	EMPENNAGE SERVO	HITECH	HS-5065 MG

UNLESS OTHERWISE SPECIFIED:
DIMENSIONS ARE IN INCHES
TOLERANCES:
ANGULAR: ±5 °
ONE PLACE DECIMAL ±.100
TWO PLACE DECIMAL ± .030

SAMUELI SCHOOL OF ENGINEERING
UNIVERSITY of CALIFORNIA · IRVINE

UNIVERSITY OF CALIFORNIA: IRVINE
RAYTHEON - DESIGN/BUILD/FLY 2018-19
DOCUMENT TITLE:
SYSTEMS LAYOUT / LOCATION

	NAME	DATE
DRAWN BY:	M. SEVILLA	2/15/2019
CHECKED BY:	E. HERNANDEZ	2/19/2019
CHIEF ENGINEER:	N. YEUNG	2/19/2019

SIZE	APPROVAL DATE:	REPORT TITLE:	REV
B	2/19/2019	DRAWING PACKAGE	NC
	SCALE: 1:10	SHEET 3 OF 3	

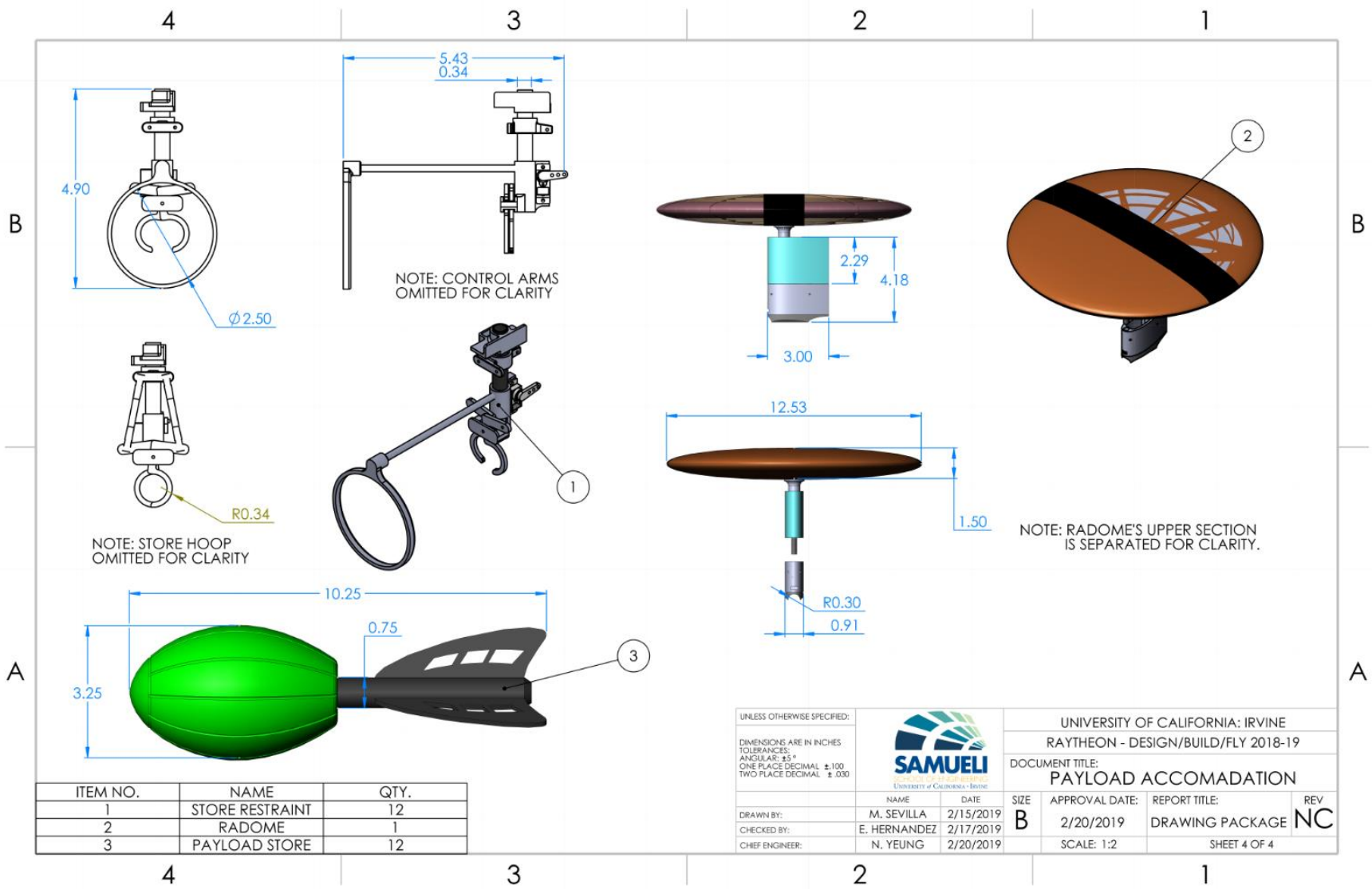
4
3
2
1
B
A
5.43
0.34
4.90
Ø2.50
NOTE: CONTROL ARMS
OMITTED FOR CLARITY
2.29
4.18
3.00
2
R0.34
NOTE: STORE HOOP
OMITTED FOR CLARITY
1
12.53
1.50
R0.30
0.91
NOTE: RADOME'S UPPER SECTION
IS SEPARATED FOR CLARITY.
10.25
0.75
3.25
3
ITEM NO. | NAME | QTY.
1 | STORE RESTRAINT | 12
2 | RADOME | 1
3 | PAYLOAD STORE | 12
UNLESS OTHERWISE SPECIFIED:
DIMENSIONS ARE IN INCHES
TOLERANCES:
ANGULAR: ±5 °
ONE PLACE DECIMAL ±.100
TWO PLACE DECIMAL ± .030
SAMUELI
SCHOOL OF ENGINEERING
University of California - Irvine
UNIVERSITY OF CALIFORNIA: IRVINE
RAYTHEON - DESIGN/BUILD/FLY 2018-19
DOCUMENT TITLE:
PAYLOAD ACCOMADATION
NAME | DATE
DRAWN BY: M. SEVILLA 2/15/2019
CHECKED BY: E. HERNANDEZ 2/17/2019
CHIEF ENGINEER: N. YEUNG 2/20/2019
SIZE B
APPROVAL DATE: 2/20/2019
REPORT TITLE: DRAWING PACKAGE
REV NC
SCALE: 1:2
SHEET 4 OF 4

6.0 Manufacturing Plan

The manufacturing plan focused on the major components of the aircraft: The manufacturing processes selected were based on the application, feasibility of manufacture, and ability to produce high quality components with available resources.

6.1 Manufacturing Processes Investigated

Balsa Structures

Balsa was selected to be the main structural material for the wing ribs and chord. This decision was made based on early prototypes of test structures. Balsa boards were quickly and inexpensively laser cut from CAD drawings to create precise parts such as wings ribs, sheeting, and stringers. The team also worked on laser cutting components including formers and stringers to construct a structural web for the radome.

3D Printing

3D Printing is a time efficient method for producing complex parts, while preserving dimensional accuracy. The team concluded that it is ideal to utilize 3D printing for making moving parts and objects with odd shapes. The team used 3D printing for the production of prototypes and final production parts for multiple mechanism including the wing locking mechanisms, store release mechanisms and motor mounts.

Composite Layups

For custom fiberglass and carbon fiber components, woven composite cloth is laid up with epoxy and vacuum bagged or molded to produce parts used for the tail surfaces, ailerons, fairings and other high stress components. This technique is useful sheeting over foam or balsa cores for light rigid parts. Laying up fiberglass onto foam cores creates a lightweight, external, structural reinforcement, which is particularly valuable for control surface manufacturing. In addition, pre-manufactured composites, particularly carbon fiber tubes have proved to make exceptional wing spars and tail booms due to their ability to be rapidly cut to length and their excellent strength to weight ratio.

Foam

Extruded Polystyrene foam was selected to be the building material that is ideal for making cores of composite wings, control surfaces, and fuselages. Generally, foam parts were shaped using a two axis CNC (Computer Numerical Control) hot wire cutter, while others were shaped using manual tools such as blades and sandpaper.

6.2 Manufacturing Processes Selection

6.2.1 Wings

Balsa and carbon fiber tubes were determined to be the optimal material to be used in the construction of the wings due to the large percentage of internal volume left free for other mechanisms such as wing locking and actuation mechanisms in addition to their light weight compared to similar foam wings. The wings are comprised of laser cut balsa ribs, which are placed into an alignment jig to ensure precise alignment and spacing during assembly. Balsa stringers and two carbon fiber tube spars provide the required torsional strength for flight. The empty space within the wings' balsa skeleton allowed for the required placement of the folding and locking mechanisms. The wing is then covered with thin, flexible balsa sheets from the leading edge to a location above and below the main spar in order to preserve the contour of the airfoil at the leading edge. The wing is then covered with Microlite™ to maintain the airfoil shape and provide torsional stiffness.

The ailerons and flaperons were constructed out of Polystyrene foam, for its low density and ease of shaping. They were cut using a CNC hot wire cutter, and then sanded to remove any imperfections. The control surfaces were then covered with fiberglass and carbon fiber cloth before being laid up with epoxy to form a durable outer shell to withstand torsion and bruises incurred during transportation and assembly.

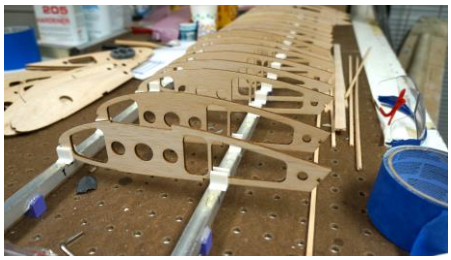

Figure 6.1: Balsa wing assembly

6.2.2 Folding Mechanism

The hinges of the wing folding mechanism, journals, and bearings guide were 3D printed from ABS filament. Actuator joints, holders, sliders, and attachment points were also 3D printed. This method allowed for custom parts to be manufactured with ease. The pivots, pulleys, and rollers were created from carbon fiber and 3D printed ABS. Carbon fiber ferrules and tubes are used for pins and lock joints. The pulley cable is comprised of Kevlar tow, which has a high tensile strength-to-weight ratio.

6.2.3 Locking Mechanism

The locking mechanisms for the folding wing tips are comprised of 3D printed parts, carbon fiber tubes, and carbon fiber ferrules. For the locking mechanism, 3D printed ABS parts were created to mount the carbon fiber locking pins and actuators to the main wing spar. With these parts firmly mounted the carbon components and actuators to the ribs and spar, as well as interfacing the actuators with sliders, the final locking mechanism is both strong and simple from maximum reliability. Carbon fiber tubes,

capable of resisting bending forces on the wing during flight, are used to house the locking pins, which are made from specialty ferrules to ensure a precise fit.

6.2.4 Radome

The radome was constructed using balsa ribs, stringers, XPS foam, and Microlite™ covering. Balsa ribs were laser cut to accurately reproduce the desired elliptical cross section and slotted into a central 3D printed hub. XPS foam was glued along the perimeter of the radome and sanded down to match the profile of the structure's leading edge. This additional structure creates a smooth and accurate leading edge as well as a clean surface to adhere covering. Additional structure was created by adding concentric balsa stringers fitted perpendicular to each rib. Finally, Microlite™ was applied to the exterior of the radome to bridge the ribs and form one cohesive outer layer.

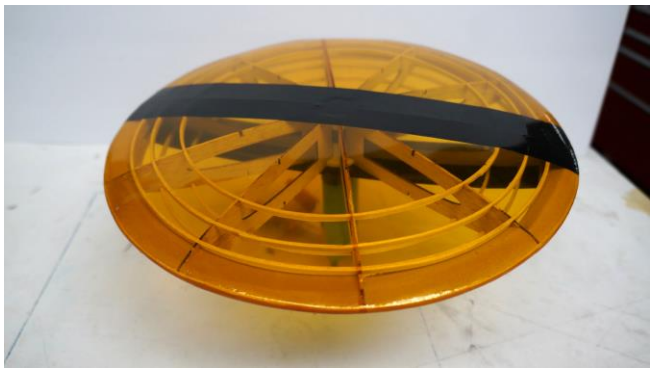

Figure 6.2: Side view of radome

6.2.5 Radome Attachment

The radome attachment is made from a set of carbon fiber tubes that runs through a 3D printed fairing structure. The shape of this component minimizes the pressure drag on the connection. Two carbon fiber tubes in the front and rear of the fairing provide structural support and a third rid with a 3D printed servo interface connect the radome to its actuator servo.

Figure 6.3: Side view of radome with attachment connected

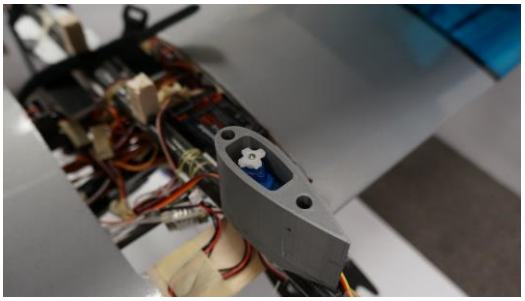

Figure 6.4: Radome mount to boom

6.2.6 Landing Gear

The primary purpose of the landing gear is to provide for a smooth and controlled transition from the runway to flight and vice versa. They must be strong enough to withstand the impact loads generated during a less than ideal landing and allow the pilot to control the aircraft on the runway even in a crosswind. The landing gear struts were created from carbon rods because of their favorable strength to weight ratio.

The main landing gear was constructed from two carbon fiber tubes anchored directly to the carbon rod of the wing spar. The carbon fiber tubes are joined to the wheels and the wing spar via custom 3D printed parts which are bonded together using CA which is idea for gluing tightly fitted components.

For the nose gear, a carbon rod is used as the strut and a carbon fiber mushroom axle mount is attached at the bottom. Layers of composite are wrapped around the mold for additional strength.

Figure 6.5: Main landing gear

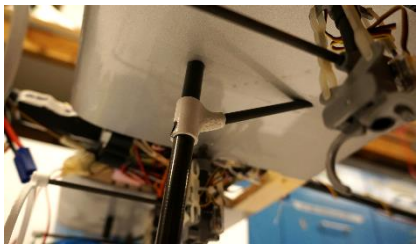

Figure 6.6: Connection between the main landing gear and wing

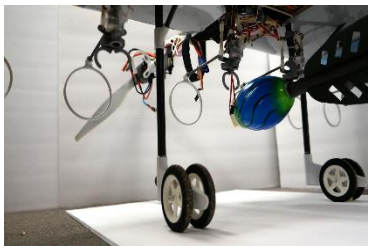

Figure 6.7: Back view of the main landing gear

Figure 6.8: Front Landing Gear

6.2.7 Store Drop Mechanism

Each individual store drop mechanism is composed of 3D printed structural housing, 3D printed claw grips, 3D printed front rings, carbon tubing and rods, and small metal pins. All 3D printed components were designed and printed to provide a custom and secure fit surrounding each store. Due to the intricate nature of the mechanism, all 3D printed components were carefully sanded to the correct dimensions and drilled to have the proper hole sizes.

The 3D printed structural housing components were attached to carbon tubing and rods using CA glue. Similarly, the carbon rod was glued to the front ring using CA glue. All of the internal components were assembled by hand within the structural housing. With the controlling sleeve placed onto the carbon tubing, pushrods could then be placed on both the claw grips and sleeve.

With the parts fully assembled, Hitec HS-40 servo motors were placed into the housing and attached to pushrods controlling the movable sleeve. After this, the entire assembly could then be fitted and glued to the carbon tube cutouts located within the wing.

Figure 6.9: Side view of store drop mechanism

Figure 6.10: front view of store drop mechanism

6.2.8 Tail Hook

The tail hook was constructed using a simple design involving the usage of a carbon fiber rod drilled vertically on the central carbon fiber boom. Attached internally to the drilled carbon fiber rod was a stainless-steel aircraft cable which elongated to the outside of the central boom via a small drilled hole. The opposite end of the cable contained a knot which allows the spotter to release the cable upon the signal of the pilot. The usage of a carbon fiber rod being drilled on to the central boom allowed for an inexpensive and little effort regarding the manufacturing of the component. Additionally,

6.3 Manufacturing Milestone Chart

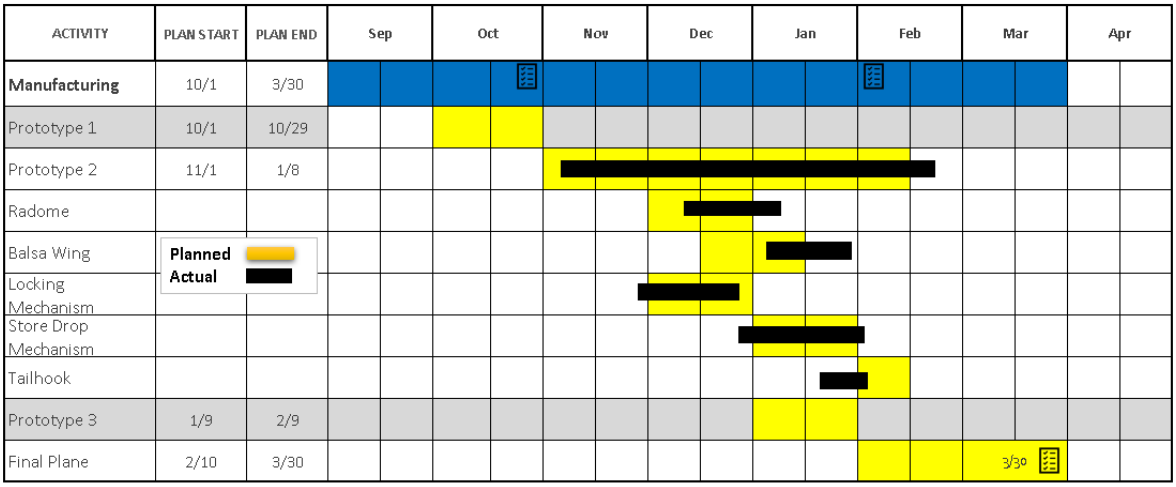

Figure 6.11: Gantt chart depicting the team's manufacturing goals and deadlines

7.0 Testing Plan

Aircraft performance was examined through various tests. Individual components, as well as, the entire aircraft were tested throughout the design process. The results revealed areas for improvement and helped guide the team in a direction towards the final design.

7.1 Objective and Schedules

The testing schedule is broken down into structural, propulsion, and flight testing, as shown in Figure 7.1. The objective of testing is to analyze key parameters of design elements and reflect upon the effectiveness of the design. The end objective is to produce a reliable and lightweight aircraft that successfully completes all missions.

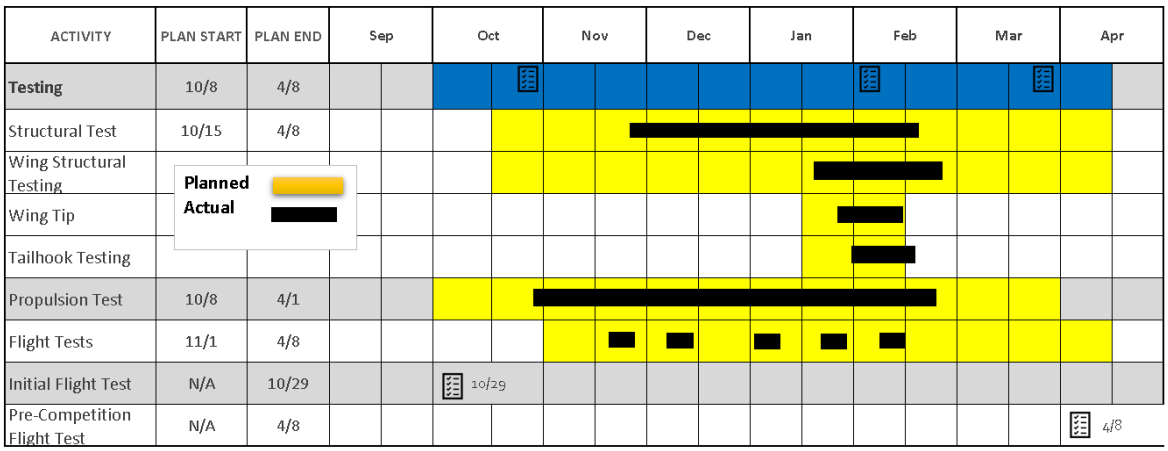

Figure 7.1: Gantt chart depicting testing objectives and schedules

7.1.1 Wing Structural Testing

Structural wing testing is emphasized due to its relevance in flight performance and packaging. Wing testing consists of torsion and bending tests. Both are probable causes for wing failure during flight. To test wing torsion, a painter's stick was glued on at the wing tip as a moment arm. A pivot point was created using a wooden stand with a metal tube placed right under the spar. A bag is attached to the end of the painter's stick with weights to induce torque. An inclinometer was then placed adjacent to the spar to measure the twist angle as weights were added incrementally. The wing is loaded and unloaded multiple times to simulate fatigue. Each loading set adds additional weight until torsional failure. Multiple trials are plotted against each other to check for permanent twisting.

To test wing bending, the wing is loaded with weight along its span. AVL gives the Cl values at each point of the wingspan, as seen in Figure 7.2. Sandbags are weighted according to the respective lift calculations and placed at the quarter-chord position of the airfoil at 3-inch stations along the span from the wing root to the wing tip. The weight placed onto the wing emulates consecutive G's of loading on the wing. The loading is done in trials to simulate fatigue testing. The amount of G's at failure and the location of the failure are recorded. When the sandbags are placed for a corresponding G loading, the deflection of the leading edge at the tip is measured for each trial. Any change in the deflection curves per trial indicates structural degradation, which may result in future wing failure. Once a wing design has been tested and reviewed, further proof testing is conducted by loading the wing up to 4G's. This ensures that the wing can withstand the required flight loads and is approved to be placed onto an aircraft.

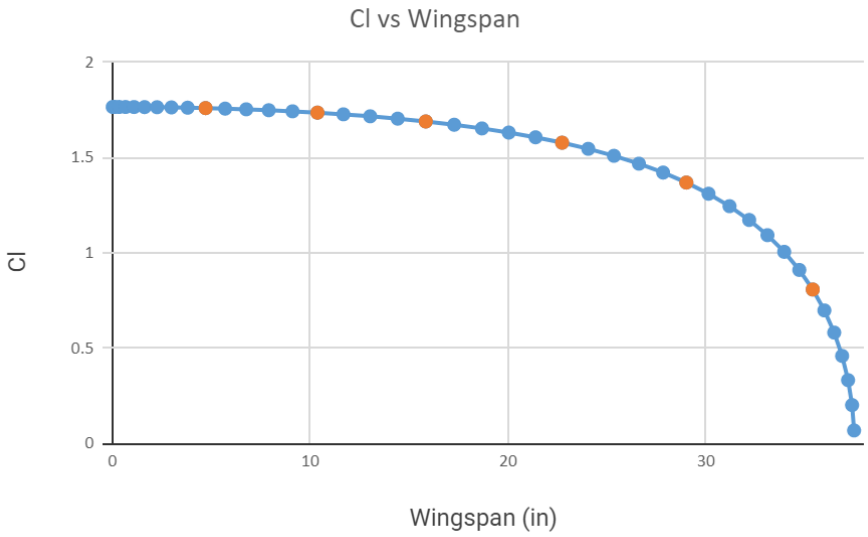

Figure 7.2: Plot of Cl vs Wingspan data collected from AVL

7.1.2 Tail Hook Structural Testing

Tail hook testing was completed with the intention to study the performance of our tail hook's connection method and cable material. Using a fish hook scale connected to the cable, a pulling force

was applied up to 30 lbs. (twice the thrust of the front propeller) to the testing setup. Different cable materials – steel wire, Kevlar string, and Kevlar tow – were tested to this standard. The success of any of the materials indicated that the hook's connection was suitable for implementation.

7.1.3 Propulsion Testing

Propulsion testing is done to analyze the motor, battery, and propeller combination performance. Static tests are done with a thrust stand by varying one component and holding all others constant. Data is recorded through the ESC attached to the motor. Testing is done by examining the watts and amps being drawn for a given static thrust requirement. The objective is to determine the relationship between different propulsion configurations. Then the configuration that produces the necessary static thrust and minimizes the battery weight required can be determined.

7.2 Pre-Flight Checklist

Pre-Flight Checklist			
Flight Date:	Wind Speed:	CG Location:	**Additional Notes:**
Flight Time:	Prototype #:	Battery Voltage:	
Location:	Takeoff Gross Weight:	Battery Used:	
Flight Inspections	Instructions: Sign off each box with initials		
Structural Integrity: Visual Inspection for Damaged Components			
Wing		**Vertical Tail**	
Fuselage		**Motor Mount**	
Landing Gear		**Motor**	
Horizontal Tail		**Propeller**	
Payload Restraints		**Control Surfaces/Pushrods**	

Avionics: Ensure Electrical Components are Properly Connected and Performing			
Motor Wiring		**Power-Up Test**	
Servo Wiring		**Range Test**	
Receiver Connected		**Receiver Battery Peaked**	
Failsafe Engaged		**Main Battery Peaked**	
Propulsion: System Should Perform as Desired			
Motor Test		**Main Battery Connected**	
Servo Test		**Receiver Battery Connected**	
Landing Gear Servo Test		**Telemetry Connected**	
Final Inspection: Final Checks Before Takeoff			
Control Surface Movement		**Objective Restated**	
Ground Crew Clear		**Pilot/Spotter Ready**	

Table 7.1: Pre-Flight Checklist

8.0 Performance Results

Each set of components was tested to improve design and validate estimated predictions. The results allow for design corrections and fine tuning of components.

A useful device that helped us gather testing data was the pixhawk. The pixhawk serves as an autopilot that enables the plane to maintain steady level flight conditions. Altitude, air speed/ground speed, and the flight path are all controlled when the device is activated. The pixhawk records acceleration, flight speed, altitude, control inputs, power, GPS, and more. The data that is collected from the pixhawk helps refine our initial power estimations to better size the battery packs. This also allows us to have a better picture of the number of stores that can be carried.

8.1 Performance of Key Subsystems

Wing and Spar Performance

Wing and spar were tested for bending moment and torsional stresses.

8.1.1 Structural Performance

Wing Loading Testing

Tip displacement was plotted versus the spanwise position to show how displacement varies with the amount of loading. The table below shows the amount of weight loaded to each section of the wing and the amount of displacement after each sandbag was placed onto the wing. A key thing to note is that the wing joint did not fail, indicating that the pin locking mechanism is sufficiently strong. The wing withstood over 4Gs and we expect the plane to experience no larger than 3Gs when flying in the competition. During the 5G test, when placing sandbag number 5, there was insufficient mounting in the test rig, the sandbags began to slide off the wing. As a result, we had to stop the test prematurely. Our goal was to have a safety factor of 1.5 and our test showed that the safety factor of the wing would be greater than 1.55, thus meeting our requirement.

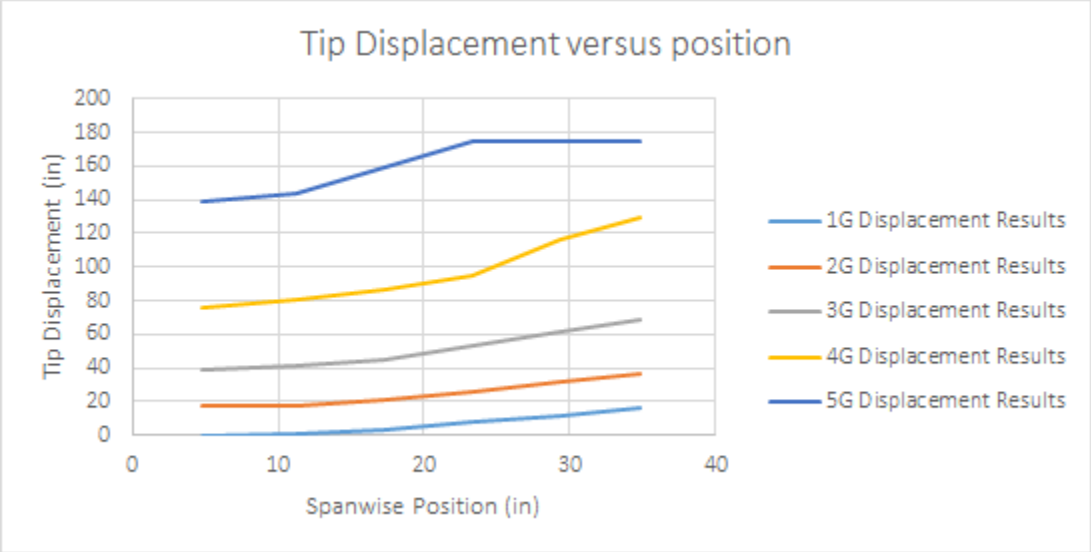

Figure 8.1: Graph depicting how tip displacement varies with the spanwise position over different amounts of loading

Distance from Center of Wing (in)	4.76	11.16	17.22	23.32	29.39	34.83	Net Moment (in-lbs)	Equivalent Gs
Load (lbs)	0.87	0.89	0.75	0.82	0.60	0.34	75.69	**1.00**
Moment (in-lbs)	4.16	9.98	12.91	19.13	17.73	11.78		
Height (in)	817.00	816.00	814.00	809.00	805.00	801.00		

Displacement (in)	0.00	1.00	3.00	8.00	12.00	16.00		
Load (lbs)	1.75	1.79	1.50	1.64	1.21	0.68	151.38	**2.00**
Moment (in-lbs)	8.31	19.95	25.83	38.26	35.45	23.56		
Height (in)	800.00	799.00	796.00	791.00	785.00	781.00		
Displacement (in)	17.00	18.00	21.00	26.00	32.00	36.00		
Load (lbs)	2.62	2.68	2.25	2.46	1.81	1.01	227.06	**3.00**
Moment (in-lbs)	12.47	29.93	38.74	57.40	53.18	35.34		
Height (in)	778.00	776.00	772.00	764.00	755.00	748.00		
Displacement (in)	39.00	41.00	45.00	53.00	62.00	69.00		
Load (lbs)	3.49	3.58	3.00	3.28	2.41	1.35	302.75	**4.00**
Moment (in-lbs)	16.63	39.91	51.66	76.53	70.91	47.13		
Height (in)	741.00	736.00	731.00	722.00	701.00	688.00		
Displacement (in)	76.00	81.00	86.00	95.00	116.00	129.00		
Load (lbs)	4.37	4.47	3.75	4.10	3.02	1.69	378.44	**5.00**
Moment (in-lbs)	20.78	49.88	64.57	95.66	88.63	58.91		
Height (in)	678.00	673.00	658.00	642.00	642.00	642.00		
Displacement (in)	139.00	144.00	159.00	175.00	175.00	175.00		

Table 8.1: Net Moment on wing

8.1.2 Propulsion Performance

For a constant power condition (simulating different sections of each mission), the thrust power and thrust data recorded was matched to static thrust data available for different propeller combinations. *Figure 8.2* illustrates a sample of the data collected during one static thrust test to determine the efficiency of a 6 cell NiMh battery while operating at its highest discharge rate.

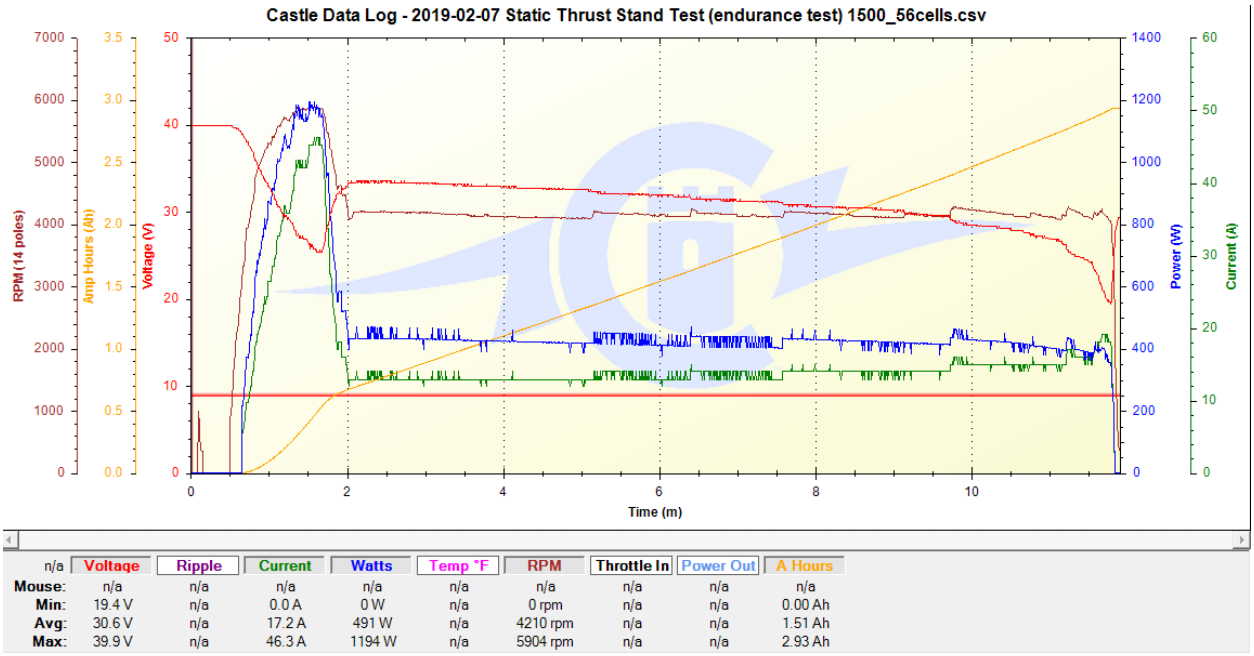

Figure 8.2: Voltage reduction of NiMH under maximum discharge load.

	Date	2/7/2019				
Stand Arm Ratio	Cell Type (mAh)	1500	5000			
1.1	# of Cells	56	28			
Motor KV	# of Packs	2	2			
275						
Propeller		Trial 1		Trial 2		
19x8 (APC)	Time (min:sec)	T_Rec [lbf]	T_Actual [lbf]	T_Rec [lbf]	T_Actual [lbf]	
	0:30	13.00	14.30	11.00	12.10	
	1:00	13.00	14.30	11.00	12.10	
	1:30	6.60	7.26	5.00	5.50	
	2:00	6.57	7.23	5.12	5.63	
	2:30	6.57	7.23	5.12	5.63	
	3:00	6.42	7.06	4.95	5.45	
	3:30	6.31	6.94	5.19	5.71	
	4:00	6.24	6.86	5.15	5.67	
	4:30	6.17	6.79	5.01	5.51	
	5:00	6.50	7.15	5.01	5.51	
	5:30	6.30	6.93	4.82	5.30	
	6:00	6.45	7.10	5.36	5.90	
	6:30	6.45	7.10	5.00	5.50	
	7:00	6.50	7.15	4.89		
	7:30	6.45	7.10	4.90		
	8:00	6.45	7.10	4.86		
	8:30	6.45	7.10	4.96		
	9:00	6.45	7.10	4.94		
	9:30	6.45	7.10	4.82		
	10:00	6.45	7.10	4.78		

Figure 8.3: Endurance and thrust test of different battery capacities.

Data obtained from these tests have allowed the team to determine the effective capacity and efficiency of different battery configurations under load. Voltage reductions under simulated take-off conditions were reduced by approximately 8 volts. This directly corresponded to an improved endurance of 45 seconds over the previous battery pack configuration (for the same motor, propeller, and electronic

speed controller used). For each of these battery configurations are compared to available motors and propeller combinations that maximizes endurance and thrust output. Matching the data obtained to available APC propeller data, refined estimates of the power required during flight has increased the maximum take off gross weight of the aircraft allowing the team to carry more stores.

Bibliography

[1].MIL-F-8785C. Military Specification: Flying Qualities of Piloted Airplanes, November 1980.

[2] M.V. Cook, Flight Dynamics Principles Second Ed, Reprinted 2008

[3] T. M. Foster, Dynamic Stability and Handling Qualities of Small Unmanned-Aerial-Vehicles, Brigham Young University, April 2005

[4] Hoerner, Sighard F. Fluid – Dynamic Drag. Great Britain. 1965